MID-YEAR PROGRESS REPORT
July 1, 1994

THERMOHYDRODYNAMIC ANALYSIS OF CRYOGENIC LIQUID TURBULENT FLOW FLUID FILM BEARINGS

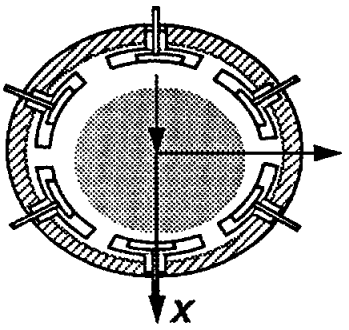

PHASE II

---

to
ational Aeronautics and Space Administration
NASA Lewis Research Center
Space Propulsion Technology Division
NASA Grant NAG3-1434

Attention: Mr. Jim Walker

by

Dr. Luis San Andres
Associate Professor

of the
Department of Mechanical Engineering
The Texas A&M University System
Texas Engineering Experiment Station

THERMOHYDRODYNAMIC ANALYSIS OF CRYOGENIC LIQUID TURBULENT FLOW FLUID FILM BEARINGS PHASE II

Period of performance: January 1994 - June 1994

Luis San Andres
Associate Professor, Texas A&M University

INDEX

THERMOHYDRODYNAMIC ANALYSIS OF CRYOGENIC LIQUID TURBULENT FLOW FLUID FILM BEARINGS
PHASE II

Period of performance: January 1994 - June 1994

Luis San Andres
Associate Professor, Texas A&M University

EXECUTIVE SUMMARY

The development of advanced analysis and computer codes for the prediction of the force response of fluid film bearings for cryogenic applications has continued on the first semester of 1994. The work in progress has extended the model and program of Phase I to include the analysis of tilting-pad and flexure-pad bearing types, as well as bearing shells with a simple elastic matrix.

Numerical solution of the bulk-flow equations within the fluid film bearing provides the bearing flow rate, load capacity, power dissipation and maximum temperature rise, and the rotordynamic force coefficients due to small amplitude journal motions. The new computer program, provisionally named as **hydroflex**, is a complex derivative of the original program **hydrosealt** delivered on March 1, 1994.

The report presents the theoretical background for the analysis of flexure pad hybrid (combination hydrostatic - hydrodynamic) bearings. The numerical predictions from the computer program are compared with test data for laminar flow tilting pad journal bearings. The application of a flexure pad orifice-compensated hybrid bearing with liquid oxygen at typical operating conditions of a cryogenic turbopump is also discussed in detail.

WORK COMPLETED ON FIRST SEMESTER of 1994

The established **original** objectives for Phase II along with a brief summary of the their current status and expected dates of completion are given below:

a) **To complete the thermohydrodynamic (THD) analysis and computer codes for design of fluid film bearings of the following types: tilting pads and flexure-pads cylindrical bearings (hydrostatic and hydrodynamic), and cylindrical pad bearings with a simple elastic matrix to model foil bearings.**

Task completed fully by Dr. Luis San Andres by July 1, 1994. See main body of this report for analysis and results.

b) **To advance the current THD model accounting for radial heat transfer through the bearing stator (sleeve).**

Analysis in progress. To be completed by Dr. L. San Andres by August 31, 1994.

c) **To provide an advanced computer code to calculate the transient fluid film bearing force response due to imposed time-varying journal displacements and velocities.**

Theoretical analysis completed on June 1, 1994.
Mr. Grigory Arauz, research assistant, will prepare the computational program and final results by October 1, 1994.

d) **To introduce a preliminary analysis for two-phase flow in annular pressure seals, and to calculate the dynamic force coefficients under these operating conditions.**

Mr. Grigory Arauz continues to review the pertinent past literature.
Theoretical analysis to be completed by November 1, 1994.

DESCRIPTION OF PROGRAM **hydroflex**

The computer program **hydroflex** is the outcome of the work for the first part of 1994. Dr. L. San Andres started developing this program since June 1993. Complete documentation on the program (Manual, Tutorial and Examples) will be ready by the end of 1994 as originally scheduled. The major advancement over the original program, **hydrosealt**, constitutes the capability for the analysis of tilting pad and flexure pad bearings, and also simple foil bearings.

In general, **hydroflex** calculates:

1) journal equilibrium position for specified load, or film forces for specified journal center displacements.
2) friction torque, power dissipation and temperature rise
3) Film moments around two axes perpendicular to journal spin axis.
4) **stiffness and damping** force coefficients due to journal center displacements and journal axis rotations
5) **stiffness and damping** moment coefficients due to journal center displacements and journal axis rotations
6) Stability indicator or whirl frequency ratio for lateral journal motions and equivalent stiffness at threshold speed of instability.
7) Complete pressure and temperature fields on the bearing surface, as well as density and viscosity field variations, within ranges of fluid flow Reynolds numbers and Mach numbers.

for

1) isothermal flow with barotropic fluid,
2) thermohydrodynamic adiabatic flow and/or isothermal journal and bearing surfaces with user specified temperatures **in the single phase flow regime.**

as a function of:

a) rotor(journal) axis misalignment.
b) inlet specified circumferential pre-swirl velocity distribution.
c) general clearance function in the axial direction, and pad preload and offset ratios.
d) simple compliance formulation to simulate foil bearings of the bending type.

and the following fluids:

1) liquid hydrogen, 2) liquid nitrogen,
3) liquid oxygen, 4) liquid methane,
5) water, 6) oil,
7) air, 8) barotropic liquid.

For liquid cryogens, the fluid properties (density, viscosity and specific heat) are calculated with the **miprops** program from NBS Standard Reference Database 12 [McCarty, 1986].

PUBLICATIONS PREPARED ON 1994

Two technical publications were prepared for the Earth to Orbit Conference at NASA Marshall Space Center last May. These papers are:

San Andres, L., and Yang, Z., **"Thermohydrodynamic Analysis of Fluid Film Bearings for Cryogenic Applications,"** 6th NASA Conference on Advanced Earth-to-Orbit Propulsion Technology, Huntsville, Alabama, May 1994.

San Andres, L., **"Analysis of Arbitrary Recess Geometry Hydrostatic Bearings,"** 6th NASA Conference on Advanced Earth-to-Orbit Propulsion Technology, Huntsville, Alabama, May 1994.

Accepted peer review journal and conference manuscripts are:

Yang, Z., L. San Andres and D. Childs, **"Thermohydrodynamic Analysis of Process Liquid Hydrostatic Bearings in Turbulent Regime, Part I: Theory, Part II: Numerical Solution and Results,"** accepted at ASME Journal of Applied Mechanics, April 1994.

Yang, Z., L. San Andres, and D. Childs, **"Process Liquid Turbulent Flow Hydrostatic Bearings: Analysis and Tests for Rotordynamic Coefficients,"** to be presented at the 4th International IFToMM Rotordynamics Conference, The Vibration Institute, Chicago, September, 1994.

Accepted for presentation at the 1994 ASME/STLE Tribology Conference Hawaii, October 1994:

Franchek, N., D. Childs, and L. San Andres, **"Theoretical and Experimental Comparisons for Rotordynamic Coefficients of a High-Speed, High-Pressure, Orifice-Compensated Hybrid Bearings,"** accepted for publication at ASME Journal of Tribology, April 1994.

Hill., D., E. Baskharone, and L. San Andres, 1993, **"Inertia Effects in a Hybrid Bearing with a 45 degree Entrance Region,"** accepted with reviews at ASME Journal of Tribology, April 1994.

San Andres, L., **"Turbulent Flow Foil Bearings for Cryogenic Applications,"** accepted with mandatory revisions at ASME Journal of Tribology, June 1994.

ANALYSIS OF FLEXURE - AND TILTING-PAD FLUID FILM BEARINGS FOR CRYOGENIC APPLICATIONS

Luis San Andres
Associate Professor
Mechanical Engineering Department
Texas A&M University
July 1, 1994

Project: Thermohydrodynamic Analysis of Cryogenic Liquid Turbulent Flow Fluid Film Bearings, PHASE II
NASA Grant NAG3-1434, TEES Project 32525-42490

Contract monitor: Mr. James Walker, NASA Lewis Research Center.

Summary

This report presents an analysis for flexure - and tilting-pad hybrid (combination hydrostatic - hydrodynamic) fluid film bearings with cryogenic liquids. Turbulent bulk-flow, variable properties, differential equations of motion govern the flow in the thin film lands of the bearing. Zeroth-order equations describe the fluid flow field for a journal static equilibrium position, and first-order linear equations govern the fluid flow for small amplitude journal center translational motions. Solution to the zeroth-order flow field equations provides the fluid film bearing flow-rate, load capacity, and torque. Solution to the first-order equations determines the linearized force coefficients due to journal radial motions. An elegant method to determine the tilting-pad moment coefficients from the force displacement coefficients is fully detailed. Also an iterative Newton-Raphson scheme to balance the pad moments is described.

For a lucid discussion on the importance and advantages of fluid film bearings in cryogenic turbomachinery see the Research Progress Report, Year I, to the present project (San Andres, 1993).

INTRODUCTION

Significant technological advances on externally pressurized bearings for cryogenic liquid applications have been achieved in the past few years. Computational design and analysis programs have been extensively correlated and validated with experimental measurements from a wealth of experimental data obtained at the TAMU Hydrostatic Bearing Test Facility (Childs and Hale, 1994). The progress achieved has also provided the necessary information to promote the use of externally pressurized, process liquid bearings for commercial high - performance rotating machinery. Advanced turbomachinery designs will soon demand an all-fluid-film-bearing technology to improve efficiency, reduce size and weight, with lesser impact on the environment. This type of machinery requires process liquid bearings for its support, and it will eliminate expensive oil-based lubrication systems as well as (anti-friction) rolling element bearings of very limited duration for high-speed applications. A relevant example of these new developments is related to magnetically driven canned and sealless pumps which in a short period of time have proven their superior performance and reliability. In other high performance applications, hydrostatic bearings and damping bearing seals are the primary candidates to provide this quantum step in machinery performance.

Despite the attractive features provided by hydrostatic journal bearings (HJBs), fluid film bearing stability considerations and thermal phenomena accompanied by fluid phase change are issues of primary concern for high speed operation with large pressure differentials (San Andres, 1993). Bearing stability is related to hydrodynamic and liquid compressibility effects which limit severely the maximum operating speed of a rotating structure to a value close to the system first critical speed divided by the whirl frequency ratio (WFR). The WFR is a stability indicator which for conventional HJBs is typically equal to 0.50. Innovative rigid bearing geometries

which improve the dynamic characteristics of HJBs have been analyzed and tested at TAMU. Some of these design configurations include rough-surface bearings, anti-swirl liquid injection HJBs, and bearings with structural stiffness asymmetry.

A promising cost-efficient alternative yet to be tested is the flexure pad HJB which conceptually should be inherently free of dynamic stability constraints (Zeidan, 1992). The major advantage of the flexure pad bearing over conventional tilt-pad technology derives from its structured design which provides the desired pad motion relative to shaft excursions without relative movement between the pad and its support, see Figure 1. Conventional tilt-pad bearings are supported on ball and socket type joints and prone to rapid wear if the fluid media has no lubricity. This is precisely the case with cryogens as well as in process liquid applications such as water. Furthermore, the flexure-pad structural arrangement allows for safe direct feeding of externally pressurized fluid to the bearing pad from which the hydrostatic action is obtained. The flexure-pad bearing technology constitutes an application of advanced automated machining processes to manufacture bearings of any specified tolerance for shape and film clearance as well as structural properties. In addition, the dynamic variation of external pressure and flow through the bearing orifice ports can lead to the concept of a **SMART BEARING**, i.e. a self-adapting, low friction, mechanical support able to modify the entire rotor-bearing system frequency response by controlling its stiffness and suppressing critical speeds.

Zeidan (1992) and Armentrout and Paquette (1993) detail the many advantages of flexure-pad bearings over conventional tilting-pad bearings. The ability of the bearing pads to rotate (about an individual pad pivot) determines a reduction or complete elimination of the undesirable cross-coupled stiffnesses which produce bearing instability in fixed geometry bearings. However, conventional tilting-pad bearings are mechanically complex due to their many parts,

and on assembly, clearance tolerances stack-up requiring a high degree of manufacturing accuracy to yield acceptable clearances. On the other hand, flexure-pad bearings are machined from a solid steel puck through an electric discharge machining (EDM) process. The thin webs are able to provide enough radial stiffness to support applied loads while still allowing for rotational pad motion to occur easily. Supply ports machined directly on the webs for delivery of pressurized lubricant offer a unique advantage over conventional and complicated delivery systems for tilting-pad hydrostatic bearings.

ANALYSIS

Consider the flow of a variable properties liquid in the thin film annular region between an inner rotating journal and a hydrostatic tilting-pad or flexure-pad bearing. The bearing pads are considered rigid in the radial (pivot) direction but provide rotational flexibility and damping, (see Figure 1). A liquid at high pressure (P_s) is supplied **radially** through orifices and flows into the bearing recesses. For hydrostatic operation, the recess pressure (P_r) is uniform over the entire recess volume, while at the recess edges, an inertial pressure drop occurs due to the sudden transition from the recess of depth (H_r) into the film land region of small thickness (H). For hybrid operation (combined hydrodynamic - hydrostatic), the pressure within the recess downstream of the supply line rises due to viscous shear effects, and closely parallels the pressure development in step bearings (Constantinescu et al., 1975, 1987). The liquid then flows into the film lands and a pressure drop to the discharge (sump) value follows. On the thin film region, hydrostatic and hydrodynamic effects are important, and for the high speed - high pressure conditions typical of cryogenic liquid environments, the fluid flow in the bearing is fully turbulent and dominated by fluid inertial effects.

The present analysis considers the fully developed turbulent bulk-flow of a cryogenic liquid whose material properties depend on its local thermophysical state of pressure and temperature. Cryogenic liquids are also characterized by low viscosities, and thermal (energy transport) effects due to friction heating and kinetic energy variations are expected to be of minor importance in the performance of hydrostatic bearings. This assertion is not fully justified for particular operating conditions (see for example Yang et al., 1993). On the other hand, due to the large levels of external pressurization required to provide substantial load capacity, the effects of pressure on the liquid properties and ultimately on bearing performance, are thought

to be of primary importance. A barotropic fluid and isothermal flow model are considered for description of the present analysis. However, the actual theoretical model includes thermal effects with solution of the energy transport equation, appropriate boundary conditions at the bearing and journal interfaces, as well as a thermal mixing model on the axial grooves between adjacent pads. The simplification used to present the analysis does not intend to diminish the importance of thermal effects in fluid film bearings for conventional or industrial applications, but rather intends to keep the complexity of the theoretical model within tolerable bounds. Details of the thermohydrodynamic model used in a similar computational development for fixed geometry bearings are given by San Andres (1993).

Coordinate system and film thickness:

A local coordinate system is placed on the unwrapped plane of the bearing with the {x,z} axes pointing in the circumferential and axial directions, respectively. This cartesian coordinate system, a fundamental assumption of lubrication theory, is a logical consequence of the smallness of the film thickness relative to the bearing diameter and length.

A characteristic tilting pad of angular extent Θ_k and axial length equal $L=L_L+L_R$ is shown in Figure 2. The leading edge of the k-th pad is defined by the coordinate Θ_{lk}, and Θ_{pk} denotes the position of the pad pivot or rotational flexural web. At operating conditions, the journal position relative to the bearing housing is described with reference to the inertial axes {X,Y,Z} by the journal center displacements (e_X,e_Y) and by the pad rotational angle (δ^k). Simple geometrical relationships determine the film thickness in the flow region of the k-th bearing pad to be given by the following expression:

$$H^k(Z,\theta,t) = C_p(Z) + e_X\cos(\theta) + e_Y\sin(\theta) - r_{pk}\cos(\theta-\Theta_p^k) - R\cdot\delta^k\sin(\theta-\Theta_p^k) \qquad (1)$$

where $\Theta=x/R$; C_p is the pad machined radial clearance, in general a function of the axial

coordinate (Z); $r_p=C_p-C_m$, corresponds to the bearing preload with C_m known as the bearing assembled clearance. Clearance functions of interest range from uniform and tapered (convergent, divergent) to discontinuous functions like steps and more complex forms of the structural wavy type. It is also noted that, in equation (1) above, the journal center displacement components (e_X,e_Y) and pad rotational angle (δ^K) are functions only of time. Note that no journal misalignment has been considered on the description of the film thickness. This omission is due only to simplicity in the presentation of the analysis.

The equations of motion

The fluid flow on the film lands of a bearing pad is considered as fully developed with a turbulent character due to the large axial pressure drop, high rotor surface speed and the low viscosity typical of cryogenic liquids. The equations of motion for the turbulent bulk-flow on the thin film land of the k-th bearing pad are given by (San Andres, 1992):

Equation of continuity:

$$\frac{\partial}{\partial t}(\rho H)^k + \frac{\partial}{\partial Z}(\rho H U_z)^k + \frac{\partial}{R\partial\theta}(\rho H U_\theta)^k = 0 \qquad (2)$$

Axial momentum equation:

$$-H^k\frac{\partial P^k}{\partial Z} = \frac{\mu}{H^k}\left\{k_z U_z\right\}^k + \frac{\partial(\rho H U_z)^k}{\partial t} + \left\{\frac{\partial(\rho H U_z U_z)}{\partial Z} + \frac{\partial(\rho H U_\theta U_z)}{R\partial\theta}\right\}^k \qquad (3)$$

Circumferential momentum equation:

$$-H^k\frac{\partial P^k}{R\partial\theta} = \frac{\mu}{H^k}\left\{k_\theta U_\theta - k_J\frac{\Omega R}{2}\right\}^k + \frac{\partial(\rho H U_\theta)^k}{\partial t} + \left\{\frac{\partial(\rho H U_z U\theta)}{\partial Z} + \frac{\partial(\rho H U_\theta U_\theta)}{R\partial\theta}\right\}^k \qquad (4)$$

$$k = 1, 2, \ldots Npad$$

on the flow region $\{-L_L \le Z \le L_R;\ \Theta_{lk} \le \theta \le \Theta_{lk}+\Theta_k\}$. The wall shear stress difference coefficients

$k_z=k_\theta=(k_J+k_B)/2$ are taken as local functions of the turbulent friction factors, Reynolds numbers and surface conditions, i.e., $k_J=f_JR_J$, $k_B=f_BR_B$ (Hirs, 1973). For cryogenic liquids such as LH2, LO2, LN2, and LCH4, the fluid properties are calculated from the Benedict-Web-Rubin equation of state as given in the standard computer program and data base of McCarty (1986).

Hydrostatic recess flow and pressure equations:

A mass conservation equation at each bearing recess of area $(l\cdot R\cdot\Theta_r)^k$ and depth H_r is defined by the global balance between the mass flow through the orifice restrictor (Q_{ro}), the mass flow into the film lands and the time rate of change of liquid mass within the recess volume V_r. This equation is given as:

$$Q_{ro}^k = A_O\sqrt{2\,\rho_r(P_s-P_r)^k} = \int_{\Gamma_r}\left[\rho H\,\vec{U}.\vec{n}\right]^k d\,\Gamma_r + \frac{\rho_r^k\,\partial\,V_r^k}{\partial\,t} + \rho_r^k\,V_r^k\,\beta\,\frac{\partial\,P_r^k}{\partial\,t} \qquad (5)$$

$$for\quad r = 1,2,\ldots Nrecess\ in\ k\text{-}th\ pad$$

where $A_o=C_d\pi d^2/4$ is the effective orifice area and $\beta=(1/\rho)\partial\rho/\partial P$ is the fluid compressibility material coefficient at the recess volume. Γ_r represents the perimeter of the recess volume with the film lands, and with normal **n** along this boundary line.

Note that the orifice flow equation is valid only for small changes of the liquid density, and probably a more accurate relationship should be used for large variations in fluid material properties across the orifice. Such a fundamental relationship is yet unknown for compressible cryogenic liquids, although a general thermophysical model is available in the literature (Hall et al., 1986). In (5) above, the orifice discharge coefficient C_d is of extreme importance since experimental measurements at Texas A&M University and elsewhere have shown that numerical predictions require accurate C_d values to provide meaningful results. Needless to say that this orifice coefficient depends not only on the flow structure and Reynolds numbers, but also on the fluid tested and the closeness of the orifice to the journal surface among other things. Refer to

Kurtin et al. (1993), Franchek (1992) and Mosher (1992) for experimentally based discharge coefficients in high-pressure, high-speed water HJBs, and to Scharrer (1990) for some measurements on cryogenic liquid HJBs.

The fluid edge pressure at the entrance to the film lands is given by the superposition of viscous shear effects on the recess extent and an entrance drop due to fluid inertia. Figure 3 shows the assumed pressure distribution within the recess volume and details the relevant nomenclature. On the circumferential direction, the pressure rise (P_e^-) downstream of the recess orifice is given as (Constantinescu et al., 1975, 1987, San Andres, 1992):

$$\left[P_e^- = P_r - \mu_r \kappa_r \frac{R \cdot \Theta_r}{2H_r^2} \left[U_\theta (\rho_e^- / \rho_r) \eta - \frac{\Omega . R}{2} \right] \frac{1}{(1-M^2)} \right]^k \qquad (6)$$

$$r = 1, 2, \ldots N_{rec} \text{ on } k\text{-th pad}$$

where, **M** is the circumferential flow local Mach number at the orifice discharge and defined as the ratio between the azimuthal velocity U_θ and the liquid sound speed ($1./\sqrt{[\beta \rho_r]}$).

The entrance pressures (P_e^+) to the film lands in the circumferential and axial directions are given, respectively, by:

$$\left[P_e^+ = P_e^- - \frac{\rho_e^+}{2} (1+\xi_\theta) \left\{ 1 - (\rho_e^+ / \rho_e^-)^2 \, \eta^2 \right\} U_\theta^2 \right]^k \qquad (7.a)$$

$$\left[P_e^+ = P_r - \frac{\rho_e^+}{2} (1+\xi_z) \left\{ 1 - (\rho_e^+ / \rho_e^-)^2 \, \eta^2 \right\} U_z^2 \right]^k \qquad (7.b)$$

$$for \; r = 1, 2, \ldots Nrecess \; on \; k\text{-th pad}$$

The analysis generalizes equations (7) for uneven empirical entrance loss factors ξ in the axial direction (Z) and also circumferentially upstream (u) and downstream (d) of the recess. The Bernoulli like pressure drop in equations (7) occurs only if fluid flows from the recess towards the film lands. If on the contrary, fluid enters from the film lands into the bearing recess, then the edge pressure is equal to the recess pressure. This consideration is based on momentum conservation for turbulent shear flows in sudden expansions.

Boundary Conditions:

At low rotational speeds, the pressure at the side boundaries of the k-th pad is essentially constant and equal to a specified value of ambient or sump pressure, i.e.,

$$P^k(L_R,\theta)=P_R^k \;; \qquad P^k(-L_L,\theta) \;=\; P_l^k \tag{8.a}$$

and at the pad leading and trailing edges,

$$P^k(Z,\,\Theta_{lk})=P^k(Z,\,\Theta_{lk}+\Theta_k) \;=\; f_s(P_R,\,P_L) \qquad on\text{-}L_L \le Z \le L_R \tag{8.b}$$

where (f_s) denotes a linear pressure variation along the axial side of the bearing pad leading and trailing edges. At high journal surface speeds ($\Omega \cdot R$) significant momentum changes occur at the pad leading edge (Θ_{lk}). Immediately upstream of the pad, the fluid entering the film lands can develop a dynamic head equal to some fraction of a reference dynamic pressure based on the bearing surface speed (Burton and Carper, 1967, Smalley et al., 1974, Mori et al., 1991, Ettles et al., 1968), i.e.

$$\Delta P^k(Z,\,\theta_{lk}) \;=\; \frac{1}{2}\,\kappa_P \cdot \rho^k \cdot \left[\frac{\Omega \cdot R}{2}\right]^2 \tag{9}$$

The coefficient (κ_P) is an empirical (experimental) ram pressure factor. Burton and Carper (1967) suggest a value of κ_P=0.64 for high speed flows with large turbulence levels. The

appearance of this ram pressure effect at the leading edge of a bearing pad is of fundamental importance on the analysis of high speed bearings. This ram pressure is a pure inertial effect solely due to the fluid motion induced by journal rotation. The model used on the present theoretical development is very simple, although more accurate knowledge of this entrance condition would require the analysis of the complex flow field on the deep axial groove separating the bearing pads.

A further assumption about the external flow is necessary to fully specify the problem. The flow at the inlet (leading edge) to the film land in the pad bearing is assumed to be parallel to the direction of surface motion. This simplification implies that on the line,

$$-L_L \le Z \le L_R\,, \qquad U_z^k(Z, \theta_{lk}) = 0\,; \qquad k = 1\,,..,N_{pad} \tag{10}$$

This equation shows the plenum between bearing pads to act as a flow source or feeding port.

If the bearing is symmetric both in geometry and operating conditions, i.e. same axial clearance and film thickness distributions and identical pressure discharges without journal misalignment; then, the axial velocity (U_z) is null at the bearing middle plane, (Z=O). For symmetric bearings, the analysis uses effectively this condition and only solves the flow field in one-half of the bearing.

The boundary conditions noted refer only to the fluid film flow within the bearing pad. At an equilibrium journal position due to an imposed external load, each individual tilting-pad or flexure-pad must be balanced, i.e. the fluid induced moments and elastic restoring moments must add to zero. This item will be discussed later in the analysis.

Perturbation Analysis

Consider the motion of the journal as the superposition of small amplitude periodic motions around an equilibrium static position. That is, let the journal center displacements and

k-pad rotation be given by:

$$e_X(t) = e_{Xo} + \Delta e_X\, e^{i\omega t} \quad , \quad e_Y(t) = e_{Yo} + \Delta e_Y\, e^{i\omega t}$$
$$\delta^k(t) = \delta_o^k + \Delta\delta^k e^{i\omega t} \quad , \qquad i=\sqrt{-1} \tag{11}$$

where ω denotes the frequency of the whirl motion. The magnitudes of the dynamic perturbations in journal displacements and rotation, $|\{\Delta e_X, \Delta e_Y, R\cdot\Delta\delta^k\}|/C_*$, are very small (i.e. $\langle\langle\langle 1$). The film thickness can then be thought as the superposition of steady-state (h_o) and dynamic (h_1) components given by the real part of the following dimensionless expression:

$$h^k = h_o^k + h_1^k\, e^{i\omega t} \tag{12}$$

with

$$h_o^k = \bar{C}_p(z) + \varepsilon_{Xo}\cos(\theta) + \varepsilon_{Yo}\sin(\theta) - \bar{r}_p^k\cos(\theta-\Theta_p^k) - [R\cdot\delta_o^k/C_*]\sin(\theta-\Theta_p^k) \tag{13}$$

$$h_1^k = \left\{\Delta\varepsilon_X + (R/C_*)\Delta\delta^k\sin(\Theta_p^k)\right\}\cos(\theta) + \left\{\Delta\epsilon_Y - (R/C_*)\Delta\delta^k\cos(\Theta_p^k)\right\}\sin(\theta) \tag{14.a}$$

or

$$h_1 = \Delta_\alpha h_\alpha = \Delta\epsilon_X h_X + \Delta\epsilon_Y h_Y + (R/C_*)\Delta\delta^k h_\delta^k \tag{14.b}$$

with

$$h_X = \cos\theta \;; \qquad h_Y = \sin\theta,$$
$$h_\delta^k = \sin(\Theta_p^k)h_X - \cos(\Theta_p^k)h_Y = \sin(\Theta_p^k-\theta) \tag{15}$$

and

$$z = Z/R,\ \bar{C}_p = C_p(Z)/C_*,\quad \bar{r}_p = [C_p - C_m]/C_*,\qquad on\ \Theta_{lk} \le \theta \le \Theta_{lk} + \Theta_k$$

C_* is a characteristic clearance for the bearing (typically the minimum clearance on the flow region without consideration of pad preload). The functions defined in equations (14-15) greatly

facilitate the comprehension of the perturbed flow field equations and the resulting rotordynamic force coefficients given later.

For each bearing pad the flow field variables (U_z, U_θ, P), as well as the fluid properties (ρ,μ) and the shear parameters (k_θ,k_z) are also formulated as the superposition of zeroth-order and first-order complex fields describing the equilibrium condition for steady-state flow, and the perturbed condition for small amplitude dynamic journal motions, respectively. In general, these fields are expressed as:

$$\Psi^k = \Psi_o^k + e^{i\omega t}\left\{\Delta\epsilon_X\Psi_X + \Delta\epsilon_Y\Psi_Y + \Delta\delta\,(R/C_*)\Psi_\delta\right\}^k = \Psi_o^k + e^{i\omega t}\,\Delta_\alpha\,\Psi_\alpha^k \qquad \alpha = X, Y, \delta^k,\ k = 1,2,..N_{pad} \tag{16}$$

Substitution of (12-15) into the equations of motion (2-4) determines the

Zeroth-order dimensionless equations:

On film lands:

$$\frac{\partial}{\partial z}\,(\bar{\rho}_o h_o u_{zo})^k + \frac{\partial}{\partial\theta}\,(\bar{\rho}_o h_o u_{\theta o})^k = 0 \tag{17}$$

$$-h_o^k\frac{\partial p_o^k}{\partial Z} = \frac{\bar{\mu}_o}{h_o^k}\left\{k_{zo}u_{zo}\right\}^k + Re_p^*\left\{\frac{\partial}{\partial Z}\,(\bar{\rho}_o h_o u_{zo}u_{zo}) + \frac{\partial}{\partial\theta}\,(\bar{\rho}_o h_o u_{\theta o}u_{zo})\right\}^k \tag{18}$$

$$-h_o^k\frac{\partial p_o^k}{\partial\theta} = \frac{\bar{\mu}_o}{h_o^k}\left\{k_\theta u_\theta - k_J\frac{\Lambda}{2}\right\}_o^k + Re_p^*\left\{\frac{\partial}{\partial Z}\,(\bar{\rho}_o h_o u_{zo}u_{zo}) + \frac{\partial}{\partial\theta}\,(\bar{\rho}_o h_o u_{\theta o}u_{\theta o})\right\}^k \qquad k = 1,2,..,Npad \tag{19}$$

Where Re_p^* corresponds to a reference Reynolds number based on a characteristic pressure.

Refer to the Nomenclature for definition of all dimensionless variables in equations (17-19). The fluid properties are functions of its local thermophysical state, i.e. $\bar{\rho}_o = \bar{\rho}_o(p_o, T_*)$, $\bar{\mu}_o = \bar{\mu}_o(p_o, T_*)$, and where T_* is a mean bulk-flow temperature in the flow region.*

On the recess volumes of a hydrostatic bearing, the mass flow through the orifices must equal the mass flow into the bearing lands,

$$\delta_* \sqrt{\bar{\rho}_{ro}(1-p_{ro})^k} = q_{ro}^k = q_{rlo}^k = \int_{\Gamma_r} \left[\bar{\rho}_o h_o (\vec{\bar{u}}_o \cdot \vec{n}) \right]^k d\bar{\Gamma}_r \quad , \qquad (20)$$

$$for \quad r = 1, 2.. \; Nrecess \; on \; k\text{-}th \; pad$$

The circumferential pressure rise at the downstream side edge of a recess is related to the recess pressure and fluid velocity by:

$$\left[\bar{p}_{eo} = p_{ro} - \bar{\mu}_{ro} \phi_r \left(u_{\theta o} \left(\frac{\bar{\rho}_e}{\rho_r} \right) \cdot \eta - \frac{\Lambda}{2} \right) \frac{1}{(1-M^2)} \right]^k \qquad (21.a)$$

where $\phi_r = \kappa_r \Theta_r / (2 \cdot h_r^2)$ is a dimensionless recess shear factor. The recess edge-entrance film pressures in the circumferential and axial directions are given by

$$\left[p_{eo}^+ = \bar{p}_{eo}^- - \frac{\bar{\rho}_e^+}{2} \phi_\theta u_{\theta o}^2 \right]^k \qquad (21.b)$$

$$\left[p_{eo}^+ = p_{ro} - \frac{\bar{\rho}_e}{2} \phi_z u_{zo}^2 \right]^k \qquad (21.c)$$

where,

---

* In the thermal analysis including energy transport the fluid properties are functions of both pressure and temperature.

$$\phi_\theta = (1+\xi_\theta) \cdot Re_p^* \left[1 - \left[\frac{\rho_e^+}{\rho_e^-}\right] \eta^2\right] \cdot \left\{1 + \frac{1.95}{Re_H^{0.43}}\right\} \tag{21.d}$$

and

$$\phi_z = (1+\xi_z) \cdot Re_p^* \left[1 - \left[\frac{\rho_e^+}{\rho_e^-}\right] \eta^2\right]$$

Zeroth-order Boundary Conditions for a bearing pad:

At the bearing pad discharge (axial) sides and the trailing edge, the pressure takes specified values, see eqn. (8.1). The **ram** pressure jump at the leading edge of a bearing pad is given in dimensionless form as:

$$\Delta p_o^k(z, \Theta_{lk}) = \frac{1}{2} \kappa_p \cdot \bar{\rho}_o^k \cdot Re_p^* \left[\frac{\Lambda}{2}\right]^2 \tag{22.a}$$

Across the pad leading edge, $-L_L/R \le z \le L_R/R$, the flow is regarded as parallel to the bearing pad. Thus,

$$u_{zo}^k(z, \Theta_{lk}) = 0 \tag{22.b}$$

First-order dimensionless equations

The first-order flow equations for perturbations in the film thickness due to journal displacements ($\Delta e_X, \Delta e_Y$) and rotation ($\Delta\delta^k$) can be expressed in the unique form:

$$i \cdot \sigma \left\{\bar{\rho}_\alpha h_o + \bar{\rho}_o \cdot h_\alpha\right\}^k + \frac{\partial}{\partial z}\left\{\bar{\rho}_\alpha h_o u_{zo} + \bar{\rho}_o \cdot h_\alpha u_{zo} + \bar{\rho}_o h_o u_{z\alpha}\right\}^k + \frac{\partial}{\partial \theta}\left\{\bar{\rho}_\alpha h_o u_{\theta o} + \bar{\rho}_o \cdot h_\alpha u_{\theta o} + \bar{\rho}_o h_o u_{\theta\alpha}\right\}^k = 0 \tag{23}$$

$$-h_o^k \frac{\partial p_\alpha^k}{\partial z} = \left[\left\{\gamma_{zz} + i \cdot Re_s \bar{\rho}_o h_o\right\} u_{z\alpha} + \gamma_{z\theta} u_{\theta\alpha} + \gamma_{zh} h_\alpha + \gamma_{zp} \bar{\rho}_\alpha + \gamma_{z\mu} \bar{\mu}_\alpha + Re_P^* \left\{\frac{\partial}{\partial z}(\bar{\rho}_o h_o u_{zo} u_{z\alpha}) + \frac{\partial}{\partial \theta}(\bar{\rho}_o h_o u_{\theta o} u_{z\alpha}) + \bar{\rho}_o h_o \left[u_{z\alpha} \frac{\partial u_{zo}}{\partial z} + u_{\theta\alpha} \frac{\partial u_{uo}}{\partial \theta}\right]\right\}\right]^k \tag{24}$$

$$-h_o^k \frac{\partial p_\alpha^k}{\partial \theta} = \left[\{\gamma_{\theta\theta} + i \cdot Re_s \bar{\rho}_o h_o\} u_{\theta\alpha} + \gamma_{\theta z} u_{z\alpha} + \gamma_{\theta h} h_\alpha + \gamma_{\theta\rho} \bar{\rho}_\alpha + \gamma_{\theta\mu} \bar{\mu}_\alpha \right.$$

$$\left. + Re_P^* \left\{ \frac{\partial}{\partial z}(\bar{\rho}_o h_o u_{zo} u_{\theta\alpha}) + \frac{\partial}{\partial \theta}(\bar{\rho}_o h_o u_{\theta o} u_{\theta\alpha}) + \bar{\rho}_o h_o \left[u_{z\alpha} \frac{\partial u_{\theta o}}{\partial z} + u_{\theta\alpha} \frac{\partial u_{\theta o}}{\partial \theta} \right] \right\} \right]^k \tag{25}$$

for perturbations in the $\alpha = X, Y$ directions and pad rotation $\alpha = \delta^k$, $\kappa = 1, 2, \ldots Npad$.

In the equation above (h_α) correspond to the perturbation fields in film thickness as defined by equations (15). The coefficients γ_{ij}'s arise from perturbation of the shear stress factors k_x, k_θ and k_J, and their explicit formulae are given elsewhere (San Andres, 1992). For a general barotropic fluid the dynamic variations in material properties are obtained from the relations:

$$\bar{\rho}_\alpha = (\partial \bar{\rho} / \partial p)\,|_o p_\alpha, \quad \mu_\alpha = (\partial \bar{\mu} / \partial p)\,|_o p_\alpha \tag{26}$$

On each recess of a hydrostatic kth-pad bearing, the first-order continuity equation takes the linearized form:

$$-p_{r\alpha}^k \left[\frac{\delta_*^2 \bar{\rho}_{ro}}{2 q_{ro}} \{1 - \lambda_c (1 - p_{ro})\} + i \cdot \bar{\rho}_{ro} \lambda_r \cdot \lambda_{rc} \right]^k = i \cdot \bar{\rho}_{ro}^k \lambda_r \cdot h_{r\alpha}^k +$$

$$\int_{\Gamma_r} \{\bar{\rho}_o h_\alpha \bar{u}_o + \bar{\rho}_o h_o \bar{u}_\alpha + \bar{\rho}_\alpha \bar{u}_o h_o\}^k \cdot \bar{n}\, d\bar{\Gamma}_r \tag{27}$$

$$r = 1, 2 \ldots Nrecess \quad on \quad k\text{-}th \quad pad$$

The first-order recess edge (circumferential and axial) pressures into the film lands are given as

$$p_{e\alpha}^+ = p_{r\alpha}^- - \phi_\theta \left\{ \bar{\rho}_o \cdot u_{\theta o} \cdot u_{\theta\alpha} + \bar{\rho}_\alpha \frac{u_{\theta o}^2}{2} \right\}^\kappa \quad ; \quad if \quad u_{\theta o}^\kappa > 0 \tag{28.a}$$

$$p_{e\alpha}^+ = p_{r\alpha}^- - \phi_z \left\{ \bar{\rho}_o \cdot u_{zo} \cdot u_{z\alpha} + \bar{\rho}_\alpha \frac{u_{zo}^2}{2} \right\}^\kappa \quad ; \quad if \quad u_{zo}^\kappa \cdot \bar{n} > 0 \tag{28.b}$$

$$for \quad \alpha = X, Y, \delta^k$$

No perturbation on the pad leading edge ram pressure is considered. Thus, the first-order pressure field is null everywhere on the side boundaries of the bearing kth-pad: i.e. $p_\alpha^k = 0$.

Note that the first order equations, (23) to (28) can be written in the general form:

$$L\,(u_{\theta X},\ u_{zX},\ p_X,\ \rho_X,\ \mu_X)^\kappa = h_X \tag{29.a}$$

$$L\,(u_{\theta Y},\ u_{zY},\ p_Y,\ \rho_Y,\ \mu_Y)^\kappa = h_Y \tag{29.b}$$

$$L\,(u_{\theta\delta},\ u_{z\delta},\ p_\delta,\ \rho_\delta,\ \mu_\delta)^\kappa = h_\delta^\kappa = h_X \sin(\Theta_p^\kappa) - h_Y \cos(\Theta_p^\kappa) \tag{29.c}$$

where L are linear differential operators with coefficients depending only on the zeroth order flow field variables $(u_{\theta o}, u_{zo}, p_o, h_o)^k$. Note that equation (29.c) describing the perturbed flow field due to a pad rotation $(\Delta\delta^k)$ is just a linear combination of the first two equations. Hence, for homogeneous boundary conditions on the perturbed fields, the following statement is valid:

$$\Psi_\delta^k = \sin(\Theta_p^k)\ \Psi_X^k - \cos(\Theta_p^k)\ \Psi_Y^k, \quad \textit{where}\ \Psi_\delta = u_{\theta\delta},\ u_{z\delta},\ p_\delta,\ \rho_\delta,\ \mu_\delta \tag{30}$$

Equation (30) then shows that the first-order flow field due to a pad rotation can be found as the superposition of the perturbed flow fields due to journal displacements in the {X,Y} directions. This statement is important since it reduces considerably the solution time in the evaluation of the force coefficients in tilting pad bearings.

Pad Fluid Film Forces, and Dynamic Force and Moment Coefficients

Fluid film forces and moment on each bearing pad are calculated by integration of the pressure field, i.e.,

$$\begin{bmatrix} F_X^k \\ F_Y^k \end{bmatrix} = P_{sa} \cdot R^2 \cdot \int_{-L_L}^{-L_R} \int_{\Theta_{it}}^{\Theta_{it}+\Theta_t} p^k \cdot \begin{bmatrix} \cos\theta \\ \sin\theta \end{bmatrix} dz \cdot d\theta_k \quad [N] \quad , \tag{31}$$

$$k = 1, 2 \ldots N_{pad}$$

$$M^k = P_{sa} \cdot R^3 \cdot \int_{-L_L}^{-L_R} \int_{\Theta_{it}}^{\Theta_{it}+\Theta_t} p^k \cdot \sin(\theta_p^k - \theta)\, dz \cdot d\theta_k \quad [N.m] \quad , \tag{32.a}$$

$$k = 1, 2 \ldots N_{pad}$$

where P_{sa} is a characteristic pressure, $P_{sa}=P_s-P_*$ for a hydrostatic bearing, while $P_{sa}=\mu_*\Omega(R/C_*)^2$ for a hydrodynamic bearing. Note that the pad moment due to the fluid film flow can be written as:

$$M^k = R \left\{ \sin(\theta_p^k)\, F_X^k - \cos(\theta_p^k)\, F_Y^k \right\} \tag{32.b}$$

Substitution of the pressure field, (eqn. 16)

$$P^k = P_o^k + e^{i\tau} \left\{ \Delta\varepsilon_X p_X + \Delta\varepsilon_Y p_Y + \Delta\delta\,(R/C_*)\, p_\delta \right\}^k \quad , \qquad \tau = \omega t$$

into equations (31) and (32) determines the k-th pad zeroth-and first-order forces and moment due to fluid film pressure:

$$\begin{aligned} F_X^k &= F_{Xo}^k + F_{XI}^k\, e^{i\tau} = F_{Xo}^k - \left\{ Z_{XX}\, \Delta e_X + Z_{XY}\, \Delta eY + Z_{X\delta}\, \Delta\delta \right\}^k e^{i\tau} \\ F_Y^k &= F_{Yo}^k + F_{YI}^k\, e^{i\tau} = F_{Yo}^k - \left\{ Z_{YX}\, \Delta e_X + Z_{YY}\, \Delta eY + Z_{Y\delta}\, \Delta\delta \right\}^k e^{i\tau} \\ M^k &= M_o^k + M_1^k\, e^{i\tau} = M_o^k - \left\{ Z_{\delta X}\, \Delta e_X + Z_{\delta Y}\, \Delta eY + Z_{\delta\delta}\, \Delta\delta \right\}^k e^{i\tau} \end{aligned} \tag{33}$$

where

$$\begin{bmatrix} F_{Xo} \\ F_{Yo} \end{bmatrix}^k = P_{sa} \cdot R^2 \cdot \int_{-L_L}^{L_R} \int_{\Theta_{1k}}^{\Theta_{1k}+\Theta_t} p_o^k \cdot \begin{bmatrix} \cos\theta \\ \sin\theta \end{bmatrix} dz \cdot d\theta_k \tag{34}$$

and

$$M_o^k = R\left\{\sin\left(\Theta_p^k\right) F_{Xo}^k - \cos\left(\Theta_p^k\right) F_{Yo}^k\right\}$$
$$k = 1, 2 .. N_{pad} \tag{35}$$

are the zeroth order fluid film forces and induced moment for the kth-pad, respectively. The $Z_{\alpha\beta}$ are pad impedance coefficients whose real and imaginary parts correspond to pad fluid film stiffness and damping coefficients, respectively. Expressions for the pad impedance coefficients are given as:

force impedances due to journal displacements Δe_X, ΔeY:

$$Z_{\alpha\beta}^k = K_{\alpha\beta}^k + i\,\omega \cdot C_{\alpha\beta}^k = -\frac{P_{sa}R^2}{C_*} \int_{-L_L}^{L_R} \int_{\Theta_{1k}}^{\Theta_{1k}+\Theta_t} p_\beta^k h_\alpha \, dz \cdot d\theta_k \qquad \begin{matrix}[N/m] \\ \alpha, \beta = X, Y\end{matrix} \tag{36.a}$$

force impedances due to pad rotation $\Delta\delta^k$:

$$Z_{\alpha\delta}^k = K_{\alpha\delta}^k + i\,\omega \cdot C_{\alpha\delta}^k = -\frac{P_{sa}R^3}{C^2} \int_{-L_L}^{L_R} \int_{\Theta_{1k}}^{\Theta_{1k}+\Theta_t} p_\delta^k h_\alpha \, dz \cdot d\theta_k \qquad \begin{matrix}[N/rad] \\ \alpha = X, Y\end{matrix} \tag{36.b}$$

moment impedances due to journal displacements Δe_X, ΔeY:

$$Z_{\delta\beta}^k = K_{\delta\beta}^k + i\,\omega \cdot C_{\delta\beta}^k = -\frac{P_{sa}R^3}{C_*} \int_{-L_L}^{L_R} \int_{\Theta_{1k}}^{\Theta_{1k}+\Theta_t} p_\beta^k h_\delta^k \, dz \cdot d\theta \qquad \begin{matrix}[N] \\ \beta = X, Y\end{matrix} \tag{36.c}$$

moment impedance due to pad rotation $\Delta\delta^k$:

$$Z_{\delta\delta}^k = K_{\delta\delta}^k + i\,\omega \cdot C_{\delta\delta}^k = -\frac{P_{sa}R^4}{C_*} \int_{-L_L}^{L_R} \int_{\Theta_{1k}}^{\Theta_{1k}+\Theta_t} p_\delta^k h_\delta^k \, dz \cdot d\theta \qquad [N \cdot m/rad] \tag{36.d}$$

A total of 9 impedance coefficients are determined for each bearing pad. Note that since the

stiffness and damping coefficients are frequency dependent, a clear distinction of fluid inertia force or added mass coefficients is not appropriate for tilting-pad bearings. A major simplification in the evaluation of the impedance coefficients is possible by using equation (30) for the dynamic pressure field due to pad rotation, i.e.

$$p_\delta^k = \sin\left(\Theta_p^k\right) p_X^k - \cos\left(\Theta_p^k\right) p_Y^k$$

This allows the impedance coefficients to be expressed as unique functions of the force impedances $Z_{\alpha\beta}$, α, β=X,Y as follows:

$$\begin{aligned}
Z_{\delta X}^k &= R\left\{\sin\left(\Theta_p^k\right) Z_{XX}^k - \cos\left(\Theta_p^k\right) Z_{YX}^k\right\} \\
Z_{\delta Y}^k &= R\left\{\sin\left(\Theta_p^k\right) Z_{XY}^k - \cos\left(\Theta_p^k\right) Z_{YY}^k\right\} \\
Z_{X\delta}^k &= R\left\{\sin\left(\Theta_p^k\right) Z_{XX}^k - \cos\left(\Theta_p^k\right) Z_{XY}^k\right\} \\
Z_{Y\delta}^k &= R\left\{\sin\left(\Theta_p^k\right) Z_{YX}^k - \cos\left(\Theta_p^k\right) Z_{YY}^k\right\} \\
Z_{\delta\delta}^k &= R\left\{\sin\left(\Theta_p^k\right) Z_{X\delta}^k - \cos\left(\Theta_p^k\right) Z_{Y\delta}^k\right\} \\
&= R^2\left[\sin^2\left(\Theta_p^k\right) Z_{XX}^k - \sin\left(\Theta_p^k\right)\cos\left(\Theta_p^k\right)\left(Z_{XY}^k + Z_{YX}^k\right) + \cos^2\left(\Theta_p\right) Z_{YY}^k\right]
\end{aligned} \tag{37}$$

Equations (37) show only four impedance coefficients to be independent and the other five uniquely determined by the relations defined above. These equations simplify greatly the analysis of tilting-pad bearings since only the dynamic pressure fields for journal center perturbations in the {X,Y} directions are required.

Bearing Equilibrium Equation and Pad Equation of Rotational Motion

In a multiple pad bearing, the sum of the individual pad forces must balance the externally applied load W. This load has components (W_X,W_Y) on the {X,Y} directions, respectively. Thus, the static equilibrium force equation (in the absence of rotor-inertial effects) is given as:

$$W_X + \sum_{k=1}^{N_{pad}} F_X^k = 0\,; \quad W_Y + \sum_{k=1}^{N_{pad}} F_Y^k = 0 \tag{38}$$

The equation of rotational motion for each bearing pad is given as:

$$I_k \ddot{\delta}^k + \dot{C}_r^k \dot{\delta}^k + Kr_k \delta^k = M^k = R\left\{\sin\left(\Theta_p^k\right) F_X^k - \cos\left(\Theta_p^k\right) F_Y^k\right\} \tag{39}$$

$$k = 1, \ldots N_{pad}$$

Where I_k, Cr_k, Kr_k correspond to the pad inertia, and pad rotational viscous damping and structural stiffness coefficients, respectively. (Note that in a conventional tilting pad bearing, $Kr_k=0$.

A static load W_o imposed on the fluid film bearing determines a bearing equilibrium position at a static journal eccentricity (e_{Xo}, e_{Yo}) and a set of stationary pad rotations $\{\delta_o\}^k$, for $k=1,..N_{pad}$. Hence, the bearing force and pad moments equilibrium equations are given as:

$$0 = W_{Xo} + \sum_{k=1}^{N_{pad}} F_{Xo}^k\left(e_{Xo}, e_{Yo}, \delta_o^k\right) \;;$$

$$0 = W_{Yo} + \sum_{k=1}^{N_{pad}} F_{Yo}^k\left(e_{Xo}, e_{Yo}, \delta_o^k\right) \tag{40}$$

$$0 = -Kr_k \delta_o^k + M_o^k = -Kr_k \delta_o^k + R\left\{\sin\left(\Theta_p^k\right) F_{Xo}^k - \cos\left(\Theta_p^k\right) F_{Yo}^k\right\} \tag{41}$$

$$k = 1, 2, \ldots, N_{pad}$$

In the practical analysis of tilting-pad bearings, **reduced** bearing stiffness and damping

coefficients are determined at the static equilibrium position and for a particular frequency of excitation, typically synchronous ($\omega=\Omega$) or subsynchronous ($\omega<\Omega$). For small amplitude journal motions (Δe_X, Δe_Y)$e^{i\omega t}$, and pad rotations ($\Delta\delta^k$}$e^{i\omega t}$, k=1, N_{pad}, with frequency ω about the equilibrium position (e_{Xo}, e_{Yo}, $\delta^k{}_o$), the individual pad forces and the pad moment equation can be written as, (see also equation (33)):

$$F_X^k(t) = F_{Xo}^k - \left\{Z_{XX}^k \Delta e_X + Z_{XY}^k \Delta e_Y + Z_{X\delta}^k \Delta\delta^k\right\} e^{i\omega t}$$
$$F_Y^k(t) = F_{Yo}^k - \left\{Z_{YX}^k \Delta e_X + Z_{YY}^k \Delta e_Y + Z_{Y\delta}^k \Delta\delta^k\right\} e^{i\omega t} \qquad (42)$$

$$O = Kr_k\,\delta_o^k - M_o^k = \left[\left\{Kr_k - \omega^2 I_k + i\omega C_{rk}\right\}\Delta\delta^k + Z_{\delta X}^k \Delta e_X + Z_{\delta Y}^k \Delta e_Y + Z_{\delta\delta}^k \Delta\delta^k\right] e^{i\omega t} \qquad (43)$$
$$k = 1, \ldots Npad$$

Where $Z_{\alpha\beta}^k = K_{\alpha\beta} + i\,\omega\,C_{\alpha\beta}^k$ are the kth-pad impedance coefficients at frequency ω. Equations (43) indicate that the pad rotational motion is not independent of the journal dynamic displacements (Δe_X, Δe_Y).

Let

$$ZZ_{\delta\delta}^k = \left(K_{\delta\delta}^k + Kr_k - \omega^2 I_k\right) + i\,\omega\left(C_{\delta\delta}^k + Cr_k\right) \qquad (44)$$

and the relation between the k-th pad dynamic rotations and journal dynamic displacements is given as:

$$\Delta\delta^k = -\left[\frac{Z_{\delta X}}{ZZ_{\delta\delta}}\Delta e_X + \frac{Z_{\delta Y}}{ZZ_{\delta\delta}}\Delta e_Y\right]^k \qquad (45)$$

Substitution of equation (45) into the force equation (42) renders the pad reduced impedance coefficients as:

$$F_X^k(t) = F_{Xo}^k - \left[Z_{RXX}^k \Delta e_X - Z_{RXY}^k \Delta e_Y\right] e^{i\omega t}$$

$$F_Y^k(t) = F_{Yo}^k - \left[Z_{RYX}^k \Delta e_X - Z_{RYY}^k \Delta e_Y\right] e^{i\omega t} \tag{46}$$

where

$$Z_{R\alpha\beta}^k = \left[Z_{\alpha\beta} - \frac{Z_{\alpha\delta} \cdot Z_{\delta\beta}}{ZZ_{\delta\delta}}\right]^k = K_{R\alpha\beta}^k + i\,\omega\, C_{R\alpha\beta}^k \tag{47}$$

$$\alpha,\ \beta = X,\ Y$$

and, ($K^k_{R\alpha\beta}$, $C^k_{R\alpha\beta}$) are the reduced force-displacement stiffness and damping coefficients for the kth-pad. The **reduced** stiffness and damping coefficients for the entire bearing assembly are given by the summation of all the pad reduced force coefficients, i.e.

$$K_{R\alpha\beta} = \sum_{k=1}^{N_{pad}} K_{R\alpha\beta}^k; \quad C_{R\alpha\beta} = \sum_{k=1}^{N_{pad}} C_{R\alpha\beta}^k \tag{48}$$

$$\alpha,\ \beta = X,\ Y$$

Method to determine the journal static equilibrium position

A static load with components (W_{Xo}, W_{Yo}) determines the journal center equilibrium coordinates (e_{Xo},e_{Yo}) and pad rotation angles $\{\delta^k\}$, k=1,..,N_{pad}, such that equations (40) and (41) are satisfied. In practice, an iterative method is needed to determine the equilibrium journal coordinates and pad rotation angles satisfying the load and moment constraints. A Newton-Raphson algorithm is implemented in the present analysis to achieve a fast convergence to the actual solution.

Consider at iteration J, the journal center to have an eccentricity defined by its components $(e_X,e_Y)^J$ on the {X,Y} directions, and a set of pad rotational angles $\{\delta^k\}^J$, k=1,...,N_{pad} such that the pad moment equation (41) is satisfied, i.e. the pad moments are balanced. For these conditions, the bearing has a set of reduced static stiffness coefficients (calculated at ω=0) denoted as $\{K_{R\alpha\beta}\}^J$, α,β=X,Y.

New journal center coordinates $(e_X,e_Y)^{J+1}$ converging to the actual values satisfying equation (40) are determined as:

$$e_X^{J+1} = e_X^J + \Delta e_X; \quad e_Y^{J+1} = e_Y^J + \Delta e_Y \tag{49}$$

where the small changes (Δe_X, Δe_Y) are determined from solution of the equation

$$\begin{bmatrix} W_{Xo} + F_X^J \\ W_{Yo} + F_Y^J \end{bmatrix} = \begin{bmatrix} K_{RXX} & K_{RXY} \\ K_{RYX} & K_{RYY} \end{bmatrix}_J \begin{bmatrix} \Delta e_X \\ \Delta e_Y \end{bmatrix} \tag{50}$$

Improved pad rotations are found from:

$$\{\delta^K\}^{J+1} = \{\delta^K\}^J + \Delta\delta^k \ , \quad k = 1 \ , \ 2 \ldots N_{pad} \tag{51}$$

where (see also equation 45)

$$\Delta\delta^k = - \left[\frac{K_{\delta X}^k}{Kr_k + K_{\delta\delta}^k} \ \Delta e_X + \frac{K_{\delta Y}^k}{Kr_k + K_{\delta\delta}^k} \ \Delta e_Y \right]^J ; \tag{52}$$

$$k = 1 \ , \ \ldots \ , \ N_{pad}$$

Note that at each step in the iterative process the pad moment equation is satisfied, i.e.

$$\left[Kr_k \, \delta^k - M_k \right]^J = 0 \qquad k = 1 \ , \ 2 \ \ldots \ N_{pad} \tag{53}$$

The procedure continues with updated journal eccentricities and pad angles until the error in the load equation is within some predetermined range, i.e.

$$\begin{aligned} \left| W_{Xo} + F_X^J \right| &\leq \epsilon \ W_o \\ \left| W_{Yo} + F_Y^J \right| &\leq \epsilon \ W_o \end{aligned} \tag{54}$$

where ε=0.005 typically. The load-bearing equilibrium position scheme described here has proven to be quite robust for two reasons, a) at every iterative step each pad moment equation

is satisfied, and b) the improved values of journal eccentricity and pad rotation angles are predicted from the pad stiffness coefficients calculated at $\omega=0$.

At this time it is important to note that most algorithms for tilting-pad bearing analysis have difficulty in determining the journal equilibrium position when one or more pads become unloaded. ** This is most frequent for bearings with small or null preload, and the traditional approach is then to artificially increase the pad rotational angle until this becomes slightly loaded. This procedure works well for tilting-pad bearings, i.e. pads without rotational structural stiffness. On the other hand, for flexure pad bearing, if a pad becomes unloaded (null fluid film moment) then the only admissible equilibrium solution is $\delta^k=0$.

Another more difficult problem arises when a pad goes from unloaded to loaded in the current iterative step. Here unless the predicted (new) pad rotation is sufficiently large, the iterative scheme will bring the pad to a state of unloading when the actual solution indicates the opposite. The iterative scheme then introduces spurious oscillations, takes a long time and frequently gives an erroneous solution. The difficulty described can be easily overcome by recognizing that a valid equilibrium (stable) pad rotational angle requires that the pad moment stiffness be always greater than zero, i.e.

$$Kr_k+K^k_{\delta\delta} \;>\; 0 \tag{55}$$

The arguments detailed above have been incorporated into the computational analysis and improved greatly the speed of convergence to a valid solution.

** A pad is defined as unloaded (fully cavitated) when no fluid pressures (also forces and moments) are generated within the pad for the values of journal eccentricity and pad rotation angle specified. At this condition, it should be clear also that all fluid film pad stiffness coefficients are zero, in particular $K_{\delta\delta}$.

NUMERICAL SOLUTION

The well known control-volume method of Patankar (1980) is used to solve the differential equations of motion. Staggered grids containing control volumes for the primitive flow variables: circumferential and axial velocity, pressure and temperature are generated. Algebraic difference equations are derived on each control volume for the conservation of circumferential and axial momentum, and transport of energy. A discrete form of the conservation of mass equation allows determination of the pressure field. The SIMPLEC procedure of Van Doormaal and Raithby (1984) is adopted for solution of the non-linear difference equations along with a scheme for line solution developed by Launder and Leschziner (1978). Further details on the method applied to hybrid bearing configurations are given by Yang (1993).

The analysis presented earlier has considered the flow to be isothermal with a barotropic fluid. In reality, the theoretical development also considers thermal effects with an energy bulk-flow transport equation and thermal mixing at the leading edges of a bearing pad. Details of the flow equations have been omitted here for simplicity. The interested reader may found the full set of equations and analysis for the thermohydrodynamic case in a previous work by the author for fixed pad bearings (San Andres, 1993). Figure 4 shows the thermal models implemented along with the different journal and surface specified temperatures.

The numerical scheme devised to find the equilibrium solution in tilting pads and flexure pad bearings is both elegant and robust. Non-reduced force coefficients for each bearing pad are found from perturbed analytical difference equations for journal displacements in two orthogonal directions. The pad moment coefficients and force coefficients due to pad angular motions are fully defined as linear combinations of the force coefficients due to journal dynamic

displacements, see equations (37). The method then avoids numerical evaluation of moment force coefficients due to pad rotations and thus, it is fast and accurate. Recognition that the overall pad moment-rotation stiffness coefficient has to be positive for a true pad equilibrium solution brings robustness to the procedure and avoids the possibility of oscillatory solutions, in particular for unloaded pads.

RESULTS

The validity and usefulness of the analysis and computational program developed can only be assessed by extensive comparisons with relevant experimental data. In the absence of test results, comparisons with predictions from similar analysis given in the literature are then deemed necessary. In any case, the calculations from the computational model implemented can only be as good as the assumptions used in the analysis. It is noted here that the present theoretical development has as its major objective the evaluation of the force performance of cryogenic liquid fluid film bearings. This type of especial bearing application is known to require large journal surface speeds or external pressurization in order to provide the required load capacity since cryogenic liquids are essentially inviscid. Experimental results for tilting pad or flexure pad hybrid bearings handling cryogens have not been performed. Measurements of forces and force coefficients for rigid surface hybrid bearings with cryogens and surrogate fluids have appeared recently. The experimental work of Childs et al. (1994) has provided a wealth of test results and pointed out the new directions for research and uses in aerospace applications. Previous publications from the author discuss extensive comparisons with measurements obtained from the hydrostatic test facility of Childs, as well as from other relevant investigations (Butner and Murphy, 1986, Adams et al., 1992, Chaomleffel et al., 1986).

It is important to note that over the past years, the analytical work on fluid film bearings at Texas A&M University has lead both the experimental verification and the practical application of hybrid bearing technology. Many of the relevant and some times surprising analytical results have been later verified on the test stand. Most notably the issue of hydrodynamic instability in fixed geometry hybrid bearings has been known for several years. The remedies to fix or avoid this condition limiting severely the application of hybrid bearings to cryogenic turbopumps have been discussed in detail elsewhere (San Andres, 1993). Initially and without much hesitation, conventional tilting pad journal bearings with hydrostatic pressurization were proposed as ideal bearing candidates with no hydrodynamic stability restriction (Greenhill, 1991). However, the mechanical complexity of the conventional tilting pads bearing prevented its further consideration as a suitable replacement for fixed geometry hybrid bearings. More details of the drawbacks of this type of bearings are given in the introductory section of this report. The appearance of flexure pad bearings (Zeidan, 1992) on the commercial bearing market has relaxed the concerns for their potential use in cryogenic liquid turbopumps. The present technical development then presents the relevant analysis and computational predictions which demonstrate the feasibility of this type of bearing configuration for aerospace applications.

Measurements of tilting pad journal bearings force coefficients were relatively scarce in the technical literature until recently. Fundamental test results for the static and dynamic force performance of tilt-pad bearings have been reported by Someya (1988), Brockwell et al. (1990), and Parkins and Horner (1992). The detailed experimental works of Taniguchi et al. (1990), and Fillon et al. (1991) have concentrated on the static performance of tilting pad bearings under various conditions of load and shaft speed with attention to the film and pads surface temperature

evolution. These investigations have also validated comprehensive analyses for the prediction of the static performance of tilting pad bearings, and included the effects of thermal and elastic distortions of the bearing pads due to large loads, and clearance variations due to journal growth as the shaft speed increases.

The experimental work of Taniguchi et al. (1990) is most relevant to the present development since the tilting-pad bearing investigated operates both in the laminar and turbulent flow regimes. Furthermore, the measured pressure shows a "ram" effect due to fluid inertia at the leading edge of the loaded bearing pads. The THD analysis of Taniguchi et al. accounts for the effects of viscosity variation across the film thickness, includes a turbulent flow model based on the Ng and Pan Theory (1969), and a three dimensional energy transport equation for the fluid film with a differential heat conduction equation for the bearing metal. The model imposes a realistic boundary condition at the shaft interface and allows for a thermal mixing flow model at the pad leading edges. The analysis does not include thermoelastic deformations. The importance of this phenomena on tilting pad bearing performance has been clearly elucidated by Fillon et al. (1991).

Table 1 presents the geometry and operating characteristics of Taniguchi et al.(1990) four shoe tilting pad bearing. The large bearing tested (19 inches in diameter) is for use in a steam turbine and was loaded up to 300 kN (67,500 lbs). Numerical calculations using the present model have been performed using the data shown in Table 1 with an adiabatic bearing and shaft surfaces thermal model, fluid inertia at the film lands and a pad inertia entrance factor κ_p=0.25. A pad heat carry-over mixing coefficient equal to 1.0 was assumed in all the calculations. Figure 5 shows the equilibrium journal eccentricity as the load increases from 60kN to 300kN for a shaft speed of 3,000 rpm. The predicted results agree very well with the measurements

and also with the theoretical results from Taniguchi et al. (Figure 8 of referred paper). Figure 6 shows the calculated and experimental minimum film thickness for the loaded pads (2 and 3) for the same range of applied external loads. The agreement between the present numerical results and test data follows the same trend as the theoretical values provided by Taniguchi et al.

At a fixed load of 180kN and shaft speed of 3,000 rpm, Taniguchi et al. present detailed measurements of the bearing centerline pressure, film thickness and metal surface temperature. Measured frictional drag loss is equal to 200kW and the present numerical calculations predicts a similar value. The test results correspond to a (slightly) turbulent flow case with a circumferential flow Reynolds number ($\rho\Omega RC/\mu$) equal to 1,430. Figures 7 through 9 show predictions of pressure, film thickness and bulk-flow film temperature from the present model for two cases. The first case labeled as conventional shows results obtained with a model not including fluid inertia effects at the film lands or at the pads leading edges. This case corresponds to the solution of the Reynolds equation for the pressure field. The second case includes the effects of fluid inertia at the film lands and a "ram" pressure effect at the pad leading edge (κ_p=0.25). Referring to Figure 6 of Taniguchi et al. paper (1988), the present inertial flow model correlates better with the test results for pressure and film thickness. It is noted here that the numerical predictions without fluid inertia are virtually identical to those of Taniguchi et al. Recently, Fillon et al. (1991) performed similar comparisons with Taniguchi's test results and showed better agreement when accounting for the effects of elastic distortion due to thermal growth and pressure loading.

The film temperatures presented in Figure 9 are low compared with the temperature measurements at the pad bearing surface. The error is as large as 10°C for the loaded pads.

Note that the present model predicts a film bulk-flow temperature , i.e. an average temperature across the film thickness, which is certainly smaller than the measured temperatures on the bearing pads or predicted across the film thickness in a 3-dimensional model. Nonetheless, the results of the present analysis are shown to predict very well the static equilibrium journal position and provide an accurate representation of the film thickness variation with a representative distribution of the film bulk-flow temperature.

Someya's journal bearing databook (1988) is a standard reference for the design of fluid film bearings. The book details the theoretical (numerical calculations) static and dynamic force performance characteristics for a variety of fluid film bearing geometries, and includes test results for a number of relevant bearing configurations. Test bearing No. 11 of Someya's scholarly reference, namely a five shoe tilting pad bearing, has been chosen to validate the numerical predictions from the present analysis. Table 2 shows the geometric and operating characteristics of the test bearing article. Someya presents the test results in a dimensionless form as a function of a Sommerfled number defined as $S=\mu_{eff}\Omega\cdot L\cdot D\ (R/C)^2/[2\pi W]$, and where the effective viscosity is assumed to have the value corresponding to the measured fluid outlet temperature. Calculations using the present model have been performed for two flow conditions, a) an isothermal flow model without thermal energy transport and using the effective viscosity provided by Someya; and, b) an adiabatic flow model with null heat flow through the bearing and shaft surfaces, a heat carry-over mixing coefficient equal to 0.50, and an oil viscosity vs. temperature relation based on an exponential formulae. The test bearing operates on the laminar flow regime with no appreciable effects of fluid inertia at film lands or pad leading edges. The isothermal model was carried out to compare results with the analytical predictions presented by Someya (1988).

Figure 10 shows the measured and predicted equilibrium eccentricity versus the bearing Sommerfeld number. The largest Sommerfeld number (S=0.106) denotes test conditions of low load (1.2 kN) and high shaft speed (6,120 rpm), while the lowest Sommerfeld number represents the largest load (9.48kN) and lowest journal speed (2,982 rpm). The isothermal results are virtually identical to those reported by Someya (1988) in his handbook. Note that the adiabatic flow model provides better agreement with the test data for the low speed, high load condition (small S) where thermal effects are expected to be of importance.

The experimental synchronous (direct) stiffness and damping force coefficients obtained by Someya are given in Figures 11 through 14. The analytical values obtained from the isothermal flow model are similar to those from the theoretical model of Someya and not reproduced here for brevity. The figures show a different scaling from those depicted on the databook to emphasize the differences between tests and computational predictions. Figures 11 and 12 show the dimensionless direct stiffness coefficients (K_{XX},K_{YY}) versus the Sommerfeld number, respectively. The adiabatic flow model predicts better the stiffness coefficients in particular at low speeds and high loads (low Sommerfeld numbers). The large differences between the isothermal model and the adiabatic model at low S's are due to the heating of the fluid film at large loads with a calculated temperature rise as large as 100°C on the film lands. The experimental values for the direct stiffness K_{XX} are very low compared with the theoretical results. The large differences are explained in terms of both thermal and elastic deformations since the largest predicted pressure is 20.6 MPa (2,987 psi).

Figures 13 and 14 present the dimensionless damping coefficients (C_{XX}, C_{YY}) versus the Sommerfeld number. The predicted damping coefficients C_{YY} agree very well with the test data, while the other direct coefficient C_{XX} shows poor correlation at the lowest values of Sommerfeld

number (large load, low speed). The theoretical results for the adiabatic flow model correlate better and at least do not increase as the Sommerfeld number decreases.

It is noted that past analyses have generally overpredicted damping coefficients when compared to test results in tilting-pad bearings. The rationale for the large discrepancies is not yet clear as gathered from the different explanations stated in the open literature. The comparisons shown in the figures demonstrate the present theoretical model to agree well with test results for low loads and high speeds conditions. Thermoelastic deformations are a major source of discrepancy for large loads.

Experimental results for the force coefficients of flexure pad bearings are yet to appear in the literature. Zeidan (1992) and Chen (1994) describe applications in which flexure pad bearings have been shown to provide stability to otherwise unstable rotating machinery and with a performance superior to that of conventional tilting pad bearings. De Choudhury and co-workers (1992) demonstrated experimentally that a flexure-pad bearing brings a lower temperature rise and frictional power loss when compared to a similar size five shoe tilting pad journal bearing. This allowed the flexure-pad bearing to be operated at a lower oil flow while providing acceptable oil throwoff temperatures. Computations performed with the present computational program are identical to those performed by Armentrout and Paquette (1993), and Chen (1994) for flexure pad bearings operating at high speeds and light viscous fluids but still on the laminar flow regime. Typical results show, at the design load condition and as the pad rotational stiffness increases, the variation of force coefficients from a tilt-pad regime passing through a transition zone and leading to a fixed-geometry regime. Designers typically select the value of rotational stiffness which shows the least value in the difference of cross-coupled stiffness coefficients (K_{XY}-K_{YX}) just before the transition regime starts (Armentrout et al., 1993).

Then a finite element program is used to design the geometry of the flexure pad web which renders the required pad rotational stiffness as well as the pad radial stiffness when the case merits. In its simplest form, the flexure pad rotational and radial stiffness are given by the following elementary relations:

$$K_r = E \cdot I_w / h_w \ [N \cdot m/rad]; \quad K_R = A_w \cdot E / h_w \quad [N/m] \tag{56}$$

where E is the elastic modulus of the web material, h_w is the web height, $A_w = w \cdot L$ is the web cross-sectional area (of width **w** and axial length **L**), and $I_w = L \cdot w^3/12$ is the area moment of inertia. The expressions detailed do not account for the geometric stiffness due to the load applied on the pad. Note that the ratio of the radial stiffness to rotational stiffness (K_R/K_r) is equal to $12/w^2$.

The following discussion pertains to the results obtained for a flexure pad hybrid bearing for application in a liquid oxygen (LOx) turbopump. The geometry and operating conditions for the six pad bearing are given in Table 3. Each pad has a rectangular recess and an orifice fluid supply line machined across the web supporting the flexure pad. The recess to pad ratio of areas is equal to 0.236 as recommended for a LOx application (Butner and Murphy, 1986). The values of supply and discharge pressure and rotational speed correspond to that on an ALS bearing turbopump configuration. The values of axial flow, circumferential, and squeeze film flow Reynolds numbers show a turbulent flow application with large fluid inertial effects. Calculations for both an isothermal condition and an adiabatic heat flow with full pad leading edge thermal mixing were performed simultaneously. The results between both models differ little expect for an increment in fluid temperature at the pad sides of 12°K and not sufficient to affect the bearing static and dynamic performance. Henceforth, in the results that follow only the isothermal results are discussed in detail.

At the journal concentric position (e=0), Figure 15 shows the calculated whirl frequency ratio (WFR) and recess pressure ratio for increasing values of the pad rotational stiffness. The lowest value of $\mathbf{K_r}$ represents an ideal tilting pad geometry with null restraining moments, while the largest rotational stiffness effectively represents a rigid (fixed) pad bearing configuration. The effect of pad angular stiffness on the stability indicator (WFR) is clear and shows the advantage of a moving pad geometry for this high speed application. As the pad rotational stiffness increases, the recess pressure ratio decreases while the flow rate increases as shown in Figure 16. The (X) marked on this figure represents the flow rate for a conventional fixed HJB with film lands of 360° extent. Figure 17 shows the pad rotation angle (δ) and the pad minimum film thickness (occurring at the pad trailing edge) versus the pad rotational stiffness. As this stiffness increases it is obvious that the pad is unable to move and hence the minimum film thickness is that of the fixed pad. The largest rotations are expected in the tilting pad regime with a reduction in film thickness of 40%. The drag torque shown in Figure 18 is shown to decrease with the pad rotational stiffness since the effective film thickness is essentially larger. This result then shows that the flexure pad bearing has a lower frictional power than the conventional tilting pad bearing.

Figure 19 shows the synchronous force coefficients, i.e. evaluated at $\omega=\Omega$. At the concentric position, the direct coefficients are equal ($K_{XX}=K_{YY}$) while the cross-coupled coefficients differ in sign ($K_{YX}=-K_{XY}$). Note that the direct stiffnesses are about an order of magnitude larger than the cross-coupled stiffness coefficients for the fixed pad condition. The calculations show the paramount effect of the pad rotational stiffness coefficient on the rise of the cross-coupled coefficients. Figures 20 to 23 show the effect of frequency excitation on the stiffness (K_{XX}, K_{XY}), and damping (C_{XX}, C_{XY}) coefficients, respectively. The results denote

calculations at frequency ratios $f=\omega/\Omega$ equal to 0, 0.5, 1 and 2 times the rotational speed. The direct stiffness K_{XX} decreases with the frequency ratio f mainly due to fluid inertia effects, with a maximum direct stiffness at a pad rotational stiffness equal to 10,000 N·m/rad. The excitation frequency appears not to affect the cross-coupled coefficients showing then low values of cross-coupled inertia coefficients.

Next, a pad rotational stiffness ($\mathbf{K}_r$) of 10 KNm/rad was selected to perform calculations for the load capacity of the bearing at the rated operating condition. The load (W) applied to the bearing increased to a maximum of 12 kN (2,700 lbs) denoting a specific load (W/LD) equal to 3.5 MPa (507 psi). Two cases were considered, (A) load applied towards the center of a bearing pad - LOP, (B) load applied at 30° from the vertical line, i.e. between pads - LBP. Figure 24 shows the calculated journal eccentricity and the minimum film thickness occurring on the bottom pad to have a linear relationship with the applied load. Note that the smallest film thickness is just 40% of the nominal bearing clearance for the largest load applied. The selected flexure pad rotational stiffness results in a whirl frequency ratio equal to 0.25, and although not low enough to eliminate hydrodynamic instability, it constitutes a major advancement over the rigid bearing pad configuration.

The flexure pad geometry to provide the chosen value of pad rotational stiffness can be obtained using the formulae given by equation (56). Using a conventional steel with an elastic modulus of 20.7E10 N/m^2.(30E6 psi), a web height (h_w) of 1 cm and thickness (w) of 5.4 mm renders a value $\mathbf{K}_r$=10KN.m/rad. The web thickness is enough to allow for the orifice supply line of 2.581 mm diameter. The pad radial stiffness is equal to 4,135 MN/m which is an order of magnitude larger than the fluid film direct stiffness K_{XX}, and hence it affects minimally the bearing performance. (Maximum elastic web deformations of less than 3μm are expected for

the largest load applied of 12KN).

Figures 25 and 26 show the synchronous stiffness and damping coefficients versus the applied load, respectively. Note that the stiffness coefficients are virtually constant for loads to 8kN (1800 lbs). The cross-coupled stiffness coefficients for the case of load between pads (B) show the largest deviations at the largest load applied, while the direct damping coefficients decrease slightly with the applied load. The whirl frequency ratio decreases monotonically from 0.25 to 0.22 as the load increases. Figure 27 shows the calculated (dimensionless) centerline pressure and film thickness for a load of 12 kN. The largest film pressures along with minimum film occur at pad 4 where the journal load is applied. The results show a small "ram" pressure at the pads inlet, hydrodynamic pressure rises in the downstream portion of the bearing recesses along with large inertial pressure drops at the recess edges.

The analysis also includes a pad rotational damping and set to zero in all calculations presented. Flexure-pad bearings due to its automated wire-EDM construction offer the advantage of accurate specification of the gap (g) between the pad innersurface and the bearing housing. A simple one-dimensional analysis shows that the pad rotational damping is approximately equal to:

$$C_r \cong (1/60)\cdot\mu\cdot L\cdot(\Theta_p\cdot\pi D/180)^5(1/g)^3 \qquad [N\cdot m\cdot sec/rad] \qquad (57)$$

The rotational damping for a gap (g) equal to 101.6μm (0.004 mils) is equal to 0.05187 N·m·sec/rad and not large enough to affect the dynamics of the LOx flexure pad bearing. However, some commercial applications handling high viscosity lubricants may offer significant values of rotational damping. It this damping is large enough it will cause the flexure pad to become overdamped, and in fact it may lock the pads and degrade the dynamic performance of the bearing. This condition is very interesting since the flexure-pad bearing will still behave

well under static load conditions, i.e. it will show a journal displacement in the same direction as the applied load. However, the excess in rotational damping could bring hydrodynamic instability at sufficiently large speeds and whirl frequencies.

The calculations performed show that a flexure pad bearing keeps virtually all the benefits of a hydrostatic pad application (large direct stiffness and damping coefficients) while offering an accurate control on the cross-coupled stiffness coefficients and reduction in the whirl frequency ratio. The results provide ample evidence on the effects of pad rotational stiffness on the performance of a hybrid - flexure pad bearing.

CONCLUSIONS

This reports details the theoretical analysis for calculation of the dynamic force performance of tilting-pad and flexure-pad hybrid (combination hydrostatic and hydrodynamic) bearings operating in the turbulent flow regime. These types of bearings offer an alternative to improve (and eliminate) the limited stability characteristics of conventional fixed pad geometry hydrostatic bearings. In particular, a flexure pad bearing is best suited to meet this objective since it offers many advantages when compared to a conventional tilting pad bearing. These advantages encompass accuracy of manufacturing without added difficulties for assembly and calibration, adequate control of bearing preload and pad structural stiffnesses (radial and rotational), and absence of wear between shoe and pivot support. Flexure pad bearings lend themselves to a hydrostatic application since the ports for the pressurized fluid can be easily machined on the pad supporting web without added mechanical complexities and at a reduced cost.

Bulk-flow equations of mass conservation, momentum and energy transport describe the

motion of a variable properties fluid within the thin film lands of a bearing. A mass conservation equation at the recess volumes with a simple formulation for the recess pressure and temperature fields are also considered. Fluid inertia effects, temporal and adjective, are accounted for in flows with large pressure differentials or large surface speeds. Zeroth- and first-order flow equations are solved numerically to determine the flow field and calculate the pad fluid film forces and force coefficients. An elegant method to determine the journal equilibrium position and the reduced force coefficients for tilting-pad bearings is also introduced.

Numerical results from the present development have been correlated with a myriad of similar analyses for laminar flow tilting-pad bearings. Predictions from the model have also correlated well with experimental bearing static performance characteristics and dynamic force coefficients. The comparisons insure the validity of the model implemented and also widen the range of practical applications for the computational program developed.

Predictions for a flexure-pad hybrid bearing handling liquid oxygen at operating conditions typical of a turbopump applications demonstrate the ability of this type of bearing to improve the hydrodynamic stability whirl ratio, without degradation on the static load performance or reduction in direct stiffness and damping coefficients. The test example shows that hybrid bearings satisfy in excess the load requirements typical of present and future cryogenic turbopumps.

The analysis still needs to be improved in order to account for pad flexibility in the radial direction. Industrial applications where large loads are typical may also demand the inclusion of a thermoelastic model for accurate determination of pad surface temperature. These considerations may not be of great importance for a cryogenic turbopump application.

REFERENCES:

Adams, M., J. Sawicki, R. Capaldi, 1992, "Experimental Determination of Hydrostatic Journal Bearing Rotordynamic Coefficients," Proc, IMechE, Paper C432/145, pp. 365-374.

Armentrout, R. and D. Paquette, 1993, "Rotordynamic Characteristics of Flexure-Pivot Tilting Pad Journal Bearings," STLE Tribology Transactions, Vol. 36, 3, pp. 443-451.

Brockwell,K., D. Kleibub, W. Dmochowski, "Measurement and Calculation of the Dynamic Operating Characteristics of the Five Shoe, Tilting Pad Journal Bearing," STLE Tribology Transactions, Vol. 33, 4, pp. 481-492, 1990.

Burton, R.A. and J.H. Carper, 1967, "An Experimental Study of Annular Flows with Applications in Turbulent Film Lubrication," Journal of Lubrication Technology, pp. 381-391.

Butner, M., and B. Murphy, 1986, "SSME Long Life Bearings," NASA CR Report 179455.
Chaomleffel, J.P., and D. Nicholas, "Experimental Investigation of Hybrid Bearings," Tribology International, Vol. 19, 5, pp. 253-259.

Chen, W.J., 1994, "Bearing Dynamic Coefficients of Flexible Pad Bearings," accepted for presentation at ASME/STLE Tribology Conference, Hawaii, October.

Childs and K. Hale, 1994, "A Test Apparatus and Facility to Identify the Rotordynamic Coefficients of High Speed Hydrostatic Bearings," ASME Journal of Tribology, Vol. 116, 1, pp. 337-344.

Constantinescu, V.N. and S. Galetuse, 1975, "Pressure Drop Due to Inertia Forces in Step Bearings," ASME Paper 75-Lub-34.

Constantinescu, V.N. and F. DiMofte, 1987, "On the Influence of the Mach Number on Pressure Distribution in Gas Lubricated Step Bearings," Rev. Roum. Sci. Tech. - Mec. Appl., Tome 32, No. 1, pp. 51-56.

De Choudhury, P., M. Hill, and D. Paquette, "A Flexible Pad Bearing System for a High Speed Centrifugal Compressor," Proceedings of the 21st Turbomachinery Symposium, Dallas, TX, September, 1992, pp. 57-65.

Ettles, C. and A. Cameron, 1968, "Considerations of Flow Across a Bearing Groove, Journal of Lubrication Technology, pp. 312-319.

Fillon, M., J-C Bligoud, and J. Frene, "Experimental Study of Tilting-Pad Journal Bearings-Comparison with Theoretical Thermoelastohydrodynamic Results," ASME Transactions, Paper 91-trib-17.

Franchek, N., 1992, "Theory Versus Experimental Results and Comparisons for Five Recessed, Orifice Compensated, Hybrid Bearing Configurations," Texas A&M University, M.S. Thesis,

TAMU Turbomachinery Laboratories, August 1992.

Greenhill, L., 1991, Private Communication, Aerojet TechSystems Corp., CA Launder, B., and M. Leschziner, 1978, "Flow in Finite Width Thrust Bearings Including Inertial Effects," ASME Journal of Lubrication Technology, Vol. 100, pp. 330-345.

Hall, K.R., P. Eubank, J. Holste, K. Marsh, 1986, "Performance Equations for Compressible Flow Through Orifices and Other ΔP Devices: A Thermodynamics Approach," AIChe Journal, Vol. 32, No. 3, pp. 517-519.

Hirs, G.G., 1973, "A Bulk-Flow Theory for Turbulence in Lubricating Films," ASME Journal of Lubrication Technology, pp. 135-146.

Kurtin, K., Childs, D., San Andres, L.A. and K. Hale, 1993, "Experimental versus Theoretical Characteristics of a High Speed Hybrid (Combination Hydrostatic and Hydrodynamic) Bearing," ASME Journal of Tribology, Vol. 115, 2, pp. 160-169.

McCarty, R.D., 1986, NBS Standard Reference Data Base 12, Thermophysical Properties of Fluids, MIPROPS 86, Thermophysics Division, Center for Chemical Engineering, National Bureau of Standards, Colorado.

Mori, A., T. Makino and H. Mori, 1991, "Entry Flow and Pressure Jump in Submerged Multi-Pad Bearings and Grooved Bearings," ASME Paper 90-Trib-42.

Mosher, P., 1992, "Experimental vs. Experimental and Theoretical Characteristics of Five Hybrid (Combination Hydrostatic and Hydrodynamic) Bearing Designs for Use in High Speed Turbomachinery," M.S. Thesis, Texas A&M University, December.

Ng, C.W., and C. Pan, 1965, "A Linearized Turbulent Lubrication Theory," ASME Journal of Basic Engineering, Vol. 87, pp. 675-688.

Parkins, D. W., and D. Horner, "Tilting pad Journal Bearings - Measured and Predicted Stiffness Coefficients,"STLE Transactions, Pre-print No. 92-TC-3D-2.

Patankar, S., (1980), "Numerical Heat Transfer and Fluid Flow," Hemisphere Publishing Corporation, McGraw-Hill Book Company.

San Andres, L.A., 1990, "Turbulent Hybrid Bearings with Fluid Inertia Effects", ASME Journal of Tribology, Vol. 112, pp. 699-707.

San Andres, L.A., 1992, "Analysis of Turbulent Hydrostatic Bearings with a Barotropic Fluid," ASME Journal of Tribology, Vol. 114, 4, pp. 755-765.

San Andres, L.A., 1993, "Thermohydrodynamic Analysis of Cryogenic Liquid, Turbulent Flow Fluid Film Bearings," Annual Progress Report to NASA Lewis Research Center, NASA Grant NAG3-1434.

Scharrer, J.K. and R. Hibbs, 1990, "Flow Coefficients for the Orifice of a Hydrostatic Bearing," STLE Tribology Transactions, Vol. 33, pp. 543-547.

Smalley, A.J., J. H. Vohr, V. Castelli and C. Wachtmann, 1974, "An Analytical and Experimental Investigation of Turbulent Flow in Bearing Films Including Convective Fluid Inertia Forces," Journal of Lubrication Technology, pp. 151-157.

Someya, T., (editor), "Journal-Bearing Databook," Springer-Verlag, pp. 227-229, 1988.

Taniguchi, S., T. Makino, K. Takeshita, T. Ichimura, "A Thermohydrodynamic Analysis of Large Tilting-Pad Journal Bearing in Laminar and Turbulent Flow Regimes with Mixing," ASME Journal of Tribology, Vol. 112, pp. 542-549, 1990.

Van Doormal, J.P., and D. Raithby, 1984, "Enhancements of the SIMPLE Method for Predicting Incompressible Fluid Flows," Numerical Heat Transfer, Vol. 7, pp. 147-163.

Yang, Z., L. San Andres and D. Childs, 1993, "Importance of Heat Transfer from Fluid Film to Stator in Turbulent Flow Annular Seals, " WEAR, Vol. 160, pp. 269-277.

Yang, Z., 1993, "Thermohydrodynamic Analysis of Product Lubricated Hydrostatic Bearings in the Turbulent Flow Regime," Ph.D. Dissertation, Mechanical Engineering Department, Texas A&M University, December.

Zeidan, F., 1992, "Developments in Fluid Film Bearing Technology," Turbomachinery International Magazine, September/October 1992.

NOMENCLATURE

A_o	Cd $\pi d_o^2/4$. Equivalent orifice area [m^2].
Ar	$1 \cdot R_* \cdot \Theta_r$. Recess area [$m^2$].
$C_p(x), C_*, \overline{C}_p$	Radial clearance function, characteristic clearance [m], C_p/C_*.
C_m	Assembled bearing radial clearance [m].
C_{XX}^k, C_{XY}^k, C_{YX}^k, C_{YY}^k	Pad Force damping coefficients due to journal displacements [Ns/m].
$C_{\delta X}^k$, $C_{\delta Y}^k$	Pad Moment damping coefficient due to journal displacements [N-s].
$C_{\delta\delta}^k$	Pad Moment damping coefficient due to pad rotation [N-m-s.rad].
$C_{X\delta}^k$, $C_{Y\delta}^k$	Pad force damping coefficients due to pad rotation [N-s/rad].
$C_{R\alpha\beta}^k$	Reduced pad damping coefficients at frequency ω; α, β=X,Y.
$C_{R\alpha\beta}$	Reduced bearing damping coefficients; α, β=X,Y [N·s/m].
Cr_k	Pad rotational damping coefficient [N-m-s/rad].
C_d	Orifice discharge coefficient.
D	2·R. Bearing diameter [m].
d_o	Orifice discharge coefficient.
$f_{J,B}$	$a_M \left[1 + \left(c_M \frac{r_{j,B}}{H} + \frac{b_M}{R_{J,B}} \right)^{e_M} \right]$; a_M=0.001375 ; b_M=500,000 ; c_M=10,000 ; e_M=1/3.00
	Turbulent flow friction factors at journal and bearing surfaces.
F_X^k, F_Y^k	Pad fluid film forces along {X,Y} axes [N].
F_X,F_Y	Film forces along {X,Y} axes [N].
i	$\sqrt{-1}$. Imaginary unit.
I_k	Pad mass moment of Inertia [kg·m^2].

h_o	H/C*. Dimensionless zeroth-order film thickness.
h_l	$e^{i\tau}\,\Delta_\alpha\, h_\alpha$. Circumferential fluid film thickness functions.
h_X, h_Y, h_δ^k	$\cos\theta$, $\sin\theta$, $\sin(\Theta_p^k - \theta)$. Perturbed film thickness components.
H_r	Recess depth [m].
$K_{XX}^k, K_{XY}^k, K_{YX}^k, K_{YY}^k$	Pad Force stiffness coefficients due to journal displacements [N/m].
$K_{\delta X}^k, K_{\delta Y}^k$	Pad Moment stiffness coefficients due to journal displacements[N].
$K_{\delta\delta}^k$	Pad Moment stiffness coefficient due to pad rotation [N-m/rad].
$K_{X\delta}^k, K_{y\delta}^k$	Pad Force stiffness coefficients due to pad rotation [N/rad].
$K_{R\alpha\beta}^k$	Reduced pad stiffness coefficients at frequency ω; α, β=X,Y.
$K_{R\alpha\beta}$	Reduced bearing stiffness coefficients; α, β=X,Y [N/m].
Kr_k	Pad rotational structural stiffness coefficient [N·m/rad].
L, L_R, L_L	Bearing axial length = $L_R + L_L$, Right and Left axial side lengths measured from recess center [m].
l	Recess axial length [m].
M	$U_\theta \cdot \sqrt{\beta \cdot \rho_r}$. Orifice circumferential velocity Mach number.
M^k	$R\,\sin\Theta p^k\, F_X - \cos\Theta_p^k\, F_Y$. Fluid film moment on pad [N·m].
N_{pads}	Numbers of pads on bearing.
N_{recess}	Number of recesses on pad.
P,Pr	Fluid pressure, recess pressure [N/m^2].
P_e^-, P_e^+	Pressures just before and after recess edge [N/m^2].
P_L, P_R	Discharge pressures on left and right sides of bearing [N/m^2].
P_s	External supply pressure [N/m^2].
P_*	Min $\{P_L, P_R\}$. Characteristic discharge pressure [N/m^2].
P_{sa}	Characteristic pressure, = Ps-P* for hydrostatic bearings.

	$= \mu\Omega(R/C_*)^2$ for hydrodynamic bearings.
p	$(P-P_*)/(P_{sa})$. Dimensionless fluid film pressure.
p_X, p_Y, p_δ	Dimensionless dynamic (first-order) pressures.
q_{rl}	$Q_{rl}/(\rho_* U_* C_* R_*) = \int \rho \bar{h} \mathbf{u}.\mathbf{n} \cdot d\bar{\Gamma}_r$. Recess to land mass flow rate.
q_{ro}	$Q_{ro}/(\rho_* U_* C_* R_*) = \delta_* \sqrt{\rho_{ro}(1-p_{ro})}$. Orifice mass flow rate.
R	Bearing radius [m].
Re	$(\rho \cdot \Omega \cdot C \cdot R/\mu)_*$. Nominal circumferential flow Reynolds number.
Re_H	$(\rho \cdot \Omega \cdot H \cdot R/\mu)_*$. Film Reynolds number due to journal rotation.
Re_p	$(\rho \cdot U \cdot C \cdot /\mu)_*$. Reference flow Reynolds number.
Re^*_p	$Re_p \cdot (C/R)_*$. Modified reference flow Reynolds number.
Re_s	$(\rho \cdot \omega \cdot C^2/\mu)_*$. Nominal Squeeze film Reynolds number.
R_J, R_B	$(\rho/\mu) H\sqrt{[(U_\theta - \Omega \cdot R)^2 + U_z^2]}$; $(\rho/\mu) H\sqrt{[U_\theta^2 + U_z^2]}$. Flow Reynolds numbers relative to journal and bearing surfaces.
r_J, r_B	Roughness depths at journal and bearing surfaces [m].
To	Fluid film resistance torque [N-m].
T_*	Fluid mean operating temperature [°K].
U_*	$C_*^2 P_{sa}/(\mu_* R_*^2)$. Characteristic flow speed [m/s].
u_z, u_θ	$(U_z, U_\theta)/U_*$. Dimensionless bulk-flow velocities in axial and circumferential (θ) directions.
V_r	$(H_r+H)A_r+V_s$. Total recess volume [m^3].
V_s	Volume of orifice supply line [m^3].
{X,Y,Z}	Inertial coordinate system.
z	Z/R. Dimensionless axial coordinate.
$Z^k_{\alpha\beta}$	$K^k_{\alpha\beta} + i\omega C^k_{\alpha\beta}$. kth-pad impedance coefficients, α,β=X,y,δ.

$ZZ^k_{\delta\delta}$	$Kr_k + K^k_{\delta\delta} - \omega^2 I_k + i\omega\,(Cr_k + C^k_{\delta\delta})$.
$Z^k_{R\alpha\beta}$	$[ZZ_{\alpha\beta} - Z_{\alpha\delta} \cdot Z_{\delta\beta} / Z_{\delta\delta}]^k$. Pad reduced impedance coefficients, α,β=X,Y.
β	$(1/\rho)(\partial\rho/\partial P)$. Liquid compressibility coefficient [m^2/N].
δ^k	Pad rotation angle [rad].
δ_*	$\dfrac{A_o \cdot \mu_* \sqrt{2}}{c_*^3 \sqrt{\rho_* P_{sa}}}$. Dimensionless Orifice parameter.
$\varepsilon_X, \varepsilon_Y$	$(e_X, e_Y)/C_*$. Dimensionless journal eccentricities in X&Y directions.
$\Delta\varepsilon_X, \Delta\varepsilon_Y, \Delta\delta$	Dynamic (perturbed)eccentricities and pad rotation.
η	$H/(H_r+H)$. Ratio of land film thickness to recess depth.
θ	x/R. Circumferential or angular coordinate.
Θ_k	kth-pad angular length [rad].
Θ_{lk}	kth-pad angular position of pad leading edge [rad].
Θ_{pk}	kth-pad angular position of pivot [rad].
Θ^k_r	rth-recess angular length [rad] in kth-pad [rad].
$\kappa_z = \kappa_\theta$	$\dfrac{1}{2}(\kappa_J + \kappa_B)$. Turbulence shear factors in (z,θ) flow directions.
κ_J, κ_B	$f_J \cdot R_J$, $f_B \cdot R_B$. Turbulent shear parameters at journal and bearing surfaces.
κ_r	$\dfrac{Re_r^{0.681}}{7.753}$. Turbulent shear flow parameter at recess.
κ_P	Pad leading edge pressure recovery factor.
$\rho, \rho_*, \bar{\rho}$	Fluid density [Kg/m^3], characteristic density [kg/m^3], ρ/ρ_* dimensionless density.
$\mu, \mu_*, \bar{\mu}$	Fluid viscosity [Ns/m^2], characteristic viscosity [Ns/m^2], μ/μ_* dimensionless viscosity.
$\xi_{\theta u}, \xi_{\theta d}$	Empirical recess-edge entrance loss coefficients in circumferential (upstream, downstream) direction.

ξ_{zL},ξ_{zR}	Empirical recess-edge entrance loss coefficients in axial direction (left and right of recess).
λ_r	$(\omega\cdot\Theta_r\cdot l)/U_*=\omega\cdot A_r/R\cdot U_*$. Frequency parameter at recess.
λ_{rc}	$\dfrac{V_r\cdot\beta\cdot P_{sa}}{C_*\,l\cdot\Theta_r\cdot R}$. Recess volume-compressibility parameter.
λ_c	$P_{sa}\cdot\beta$. Liquid compressibility ratio.
Ω,ω	Rotational speed of journal, excitation or whirl frequency [1/s].
Λ	$\Omega\cdot R/U_*$. Dimensionless journal surface velocity parameter.
σ	$\omega\cdot R/U_*$. Film frequency parameter.
τ	ωt. Dimensionless time coordinate.
$\tau_{\theta J}$	Dimensionless shear stress at journal surface.
Γ_r	Recess boundary with outward normal $\overline{n}$.

Subscripts refer to:

z,θ	In direction of local axial and circumferential coordinates in plane of bearing.
o	Zero-th order solution.
α,β	First order solution for perturbations in (X,Y) displacements and pad rotation (δ).
r,e	Bearing recesses and edges (entrance).
L,R	Left and right axial planes of bearing.
u,d	Refers to upstream and downstream edges of recess in θ dir.

Superscripts refer to :

k	kth-pad on bearing.

Table 1. Geometry and Operating Conditions of Taniguchi et al. Bearing (1990)

Number of pads = 4
Diameter (D) = 479 mm
Length (L) = 300 mm
Clearance (C_p) = 612 μm, zero preload

Pad Arc: 80°, offset=0.50 (centrally pivoted)
pivots at 45°, 135°, 225°, 315°
Pad thickness=121 mm

Lubricant: Oil ISO VG 32 with ρ=860 kg/m^3
viscosity μ=0.0277 Pa-s at 40°C
oil viscosity-temperature coefficient 0.034 1/°C

Supply conditions: Ps=0.1 MPa at Ts=40°C
520 lit/min flow rate

Operating speed: 1krpm to 4krpm

Load between pads 2 & 3: 60kN to 300 kN.

Circumferential flow Reynolds number ($\rho\Omega RC/\mu$) = 1,430

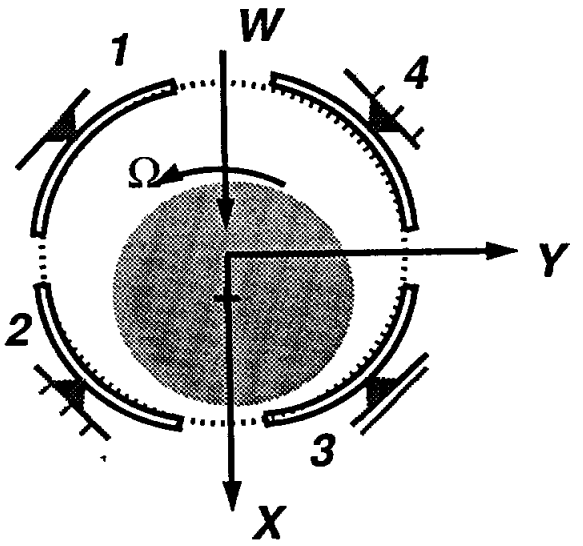

Table 2. Geometry of Test Bearing No. 11 of Someya (1988), pp. 227-229.

Number of pads = 5
Diameter (D) = 76.4 mm
Length (L) = 31.6 mm
Clearance (C_p) = 86 μm, zero preload

Pad Arc: 58°, offset=0.50 (centrally pivoted)
pivots at 36°, 108°, 180°, 252°, 324°

Lubricant: #140 turbine Oil with ρ=874 kg/m^3
viscosity ν= 61.8 mm^2/sec at 37.8°C
35.4 " 50.0°C
7.78 " 98.9°C

Supply conditions: Ps=0.1 MPa

Inlet Temperature: varies between 38.5°C to 41.3°C

Operating speed: varies between 2,980 rpm to 6,240 rpm

Load W on bottom pad (#3): 1.2 kN to 9.48 kN.

$$S = \text{Sommerfeld Number} = \frac{\mu_{eff}\,\Omega\, L\, D}{2\pi\ W}\left[\frac{R}{C_p}\right]^2$$

Dimensionless stiffness coefficients $k_{ij} = K_{ij}\ (C/W)$

damping " " $c_{ij} = C_{ij}\ (C\cdot\Omega/W)$

Refer to Someya's Databook for a detailed description of test conditions.

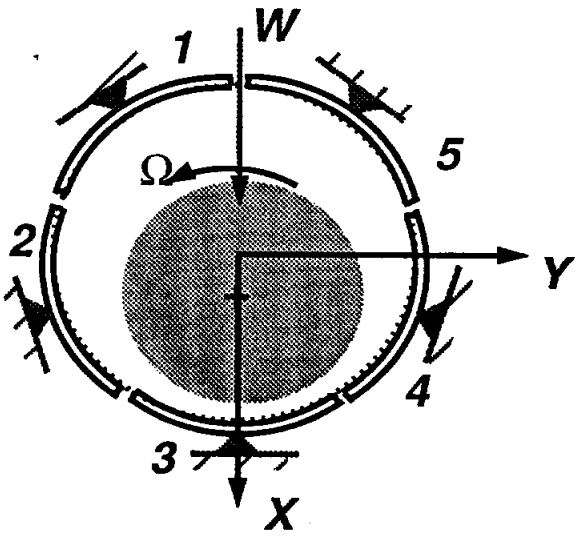

Table 3. Flexure-pad Liquid Oxygen Hybrid Bearing

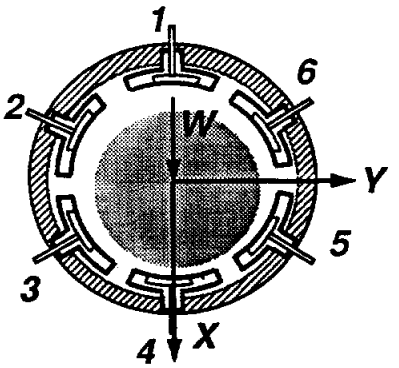

Diameter D=92.71 mm (3.65 in)
Length L=37.08 mm (1.46 in)
Clearance C_p = 76.2 μm (0.003 in), zero preload
Recess depth H_R = 228μm (0.009 in)

6 pads of length 50° and 1 recess per pad
pad offset = 0.50
pad pivots at 0°, 60°, 120°, 180°, 240°, 300°
leading edge ram pressure coefficient κ_P=0.32

recess arc length 23.5° and axial length l= 19mm (0.75 in)

orifice diameter d_o=2.58 mm, C_d=1.0

edge loss coefficients ξ_θ, ξ_y = 0.0
swirl ratio α = 0.50

Pad rotational stiffness (K_r) varies

damping (C_r) = 0 N·m·s/rad

Inertia : 1.017E-4 kg·m2, mass : 0.283 kg for thickness 0.02 m

Operating speed: 25krpm

Pressure supply	P_s = 26.71 MPa (3874 psi)
discharge	P_a = 8.81 MPa (1278 psi), ΔP= 2600 psi

Liquid oxygen at inlet temperature T_s = 90°K (162°R)

at (P_s, T_s): density ρ_s= 1,192 kg/m^3, viscosity μ_s = 0.2459E-03 Pa·s,

Reynolds numbers at concentric position,

Circumferential flow	$Re_c=(\rho/\mu)_s\Omega\cdot R\cdot C$	= 44,832
Axial flow	$Re_a=(\rho/\mu)_s V\cdot C$	= 30,487 - 30,801
Squeeze film	$Re_s=(\rho/\mu)_s\omega\cdot C^2$	= 73.52 ($\omega=\Omega$)

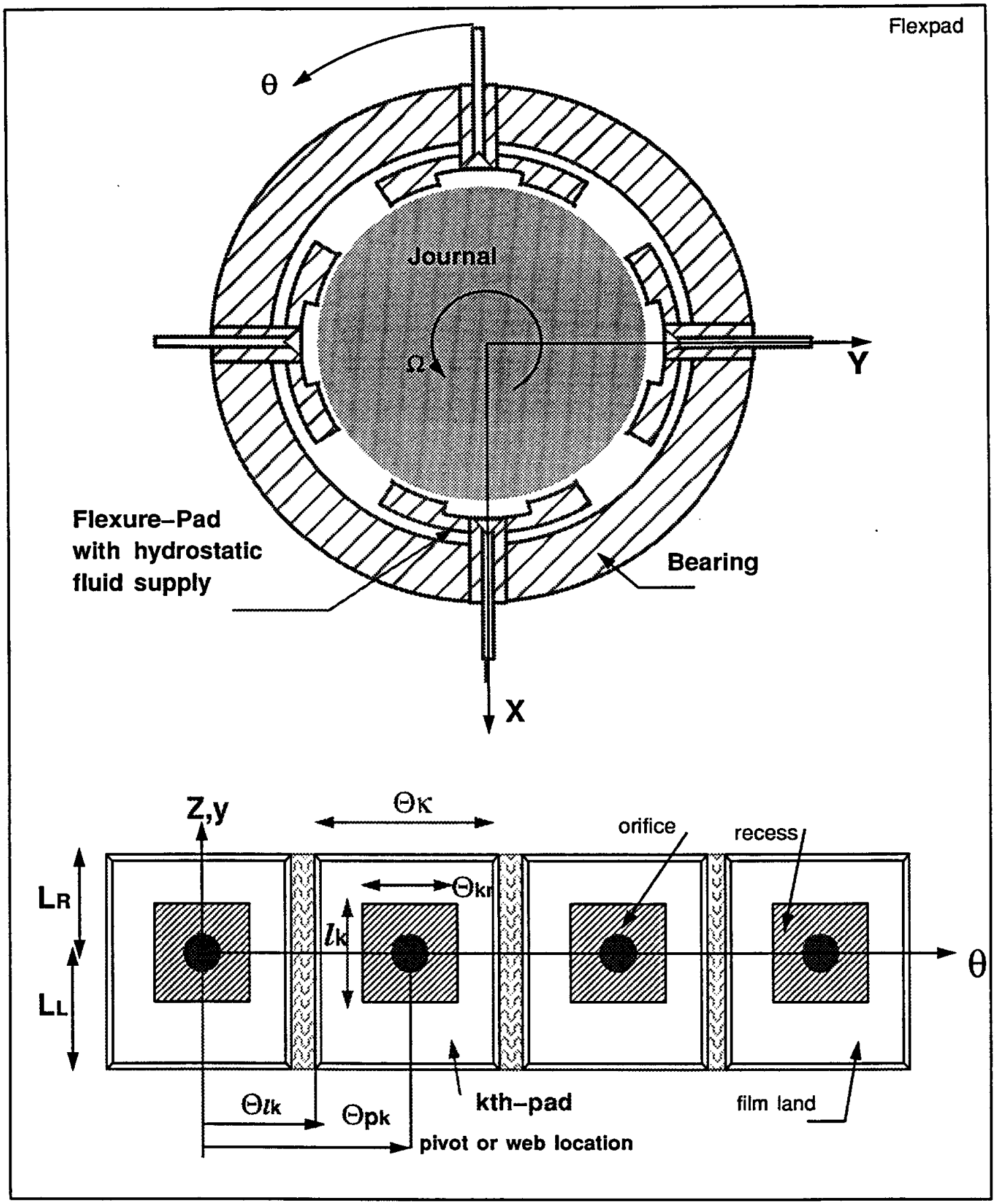

Figure 1. Geometry of flexure pad hybrid bearing

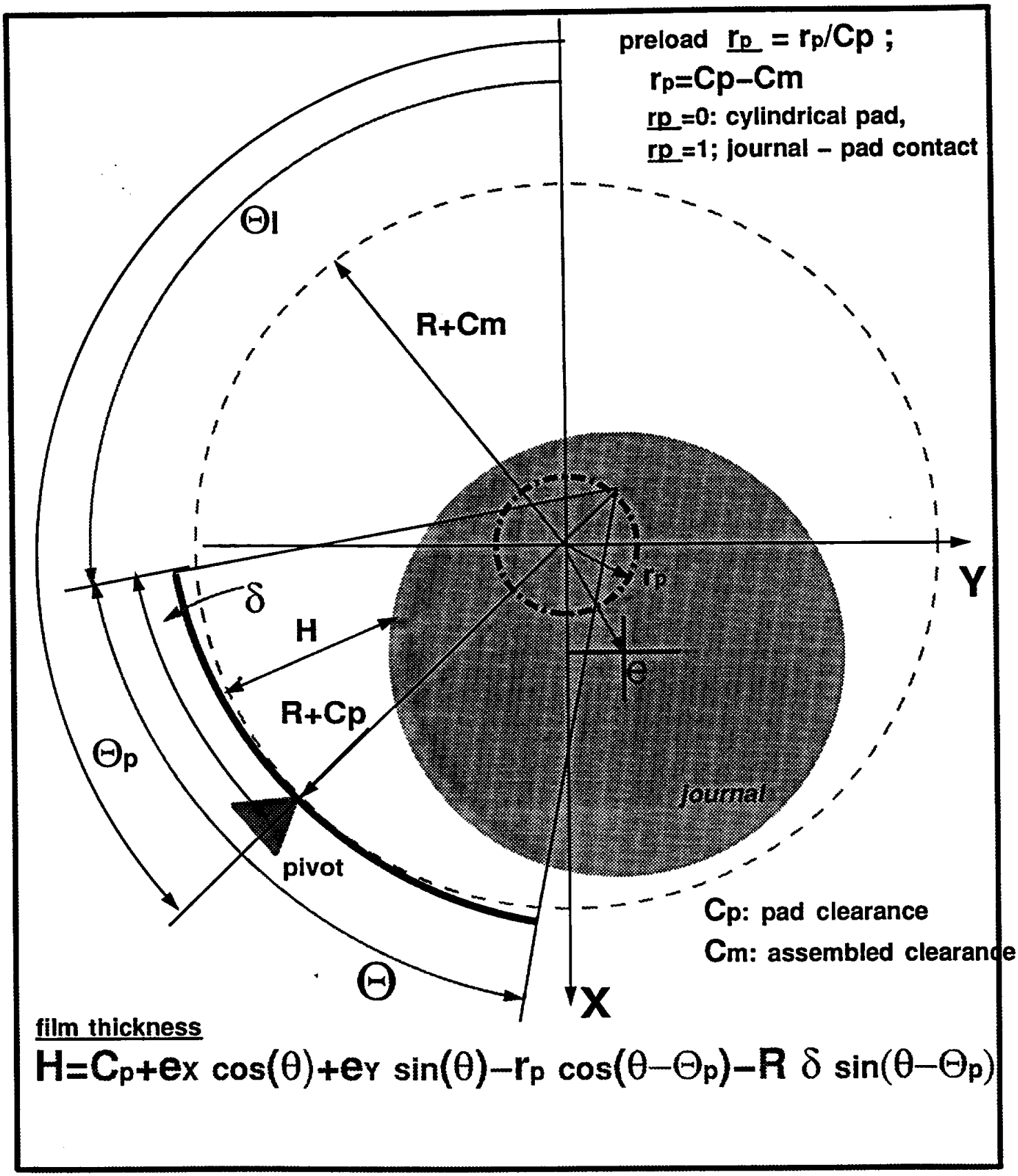

Figure 2. Geometry and nomenclature for tilting–pad

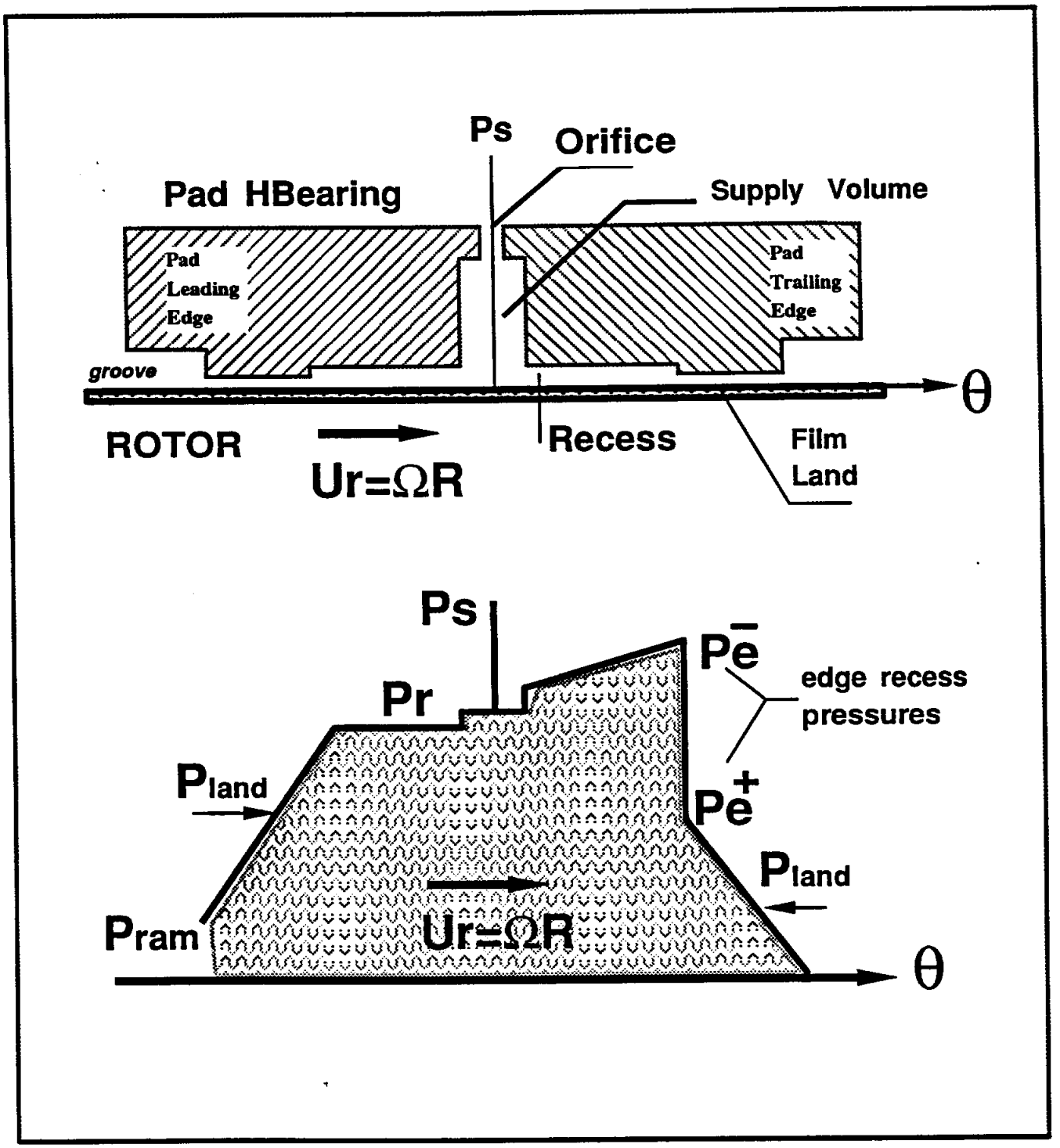

Figure 3. Conceptual description of pressure rise and drop at recess edge of a hydrostatic pad bearing, and pressure ram effect at leading edge of bearing pad..

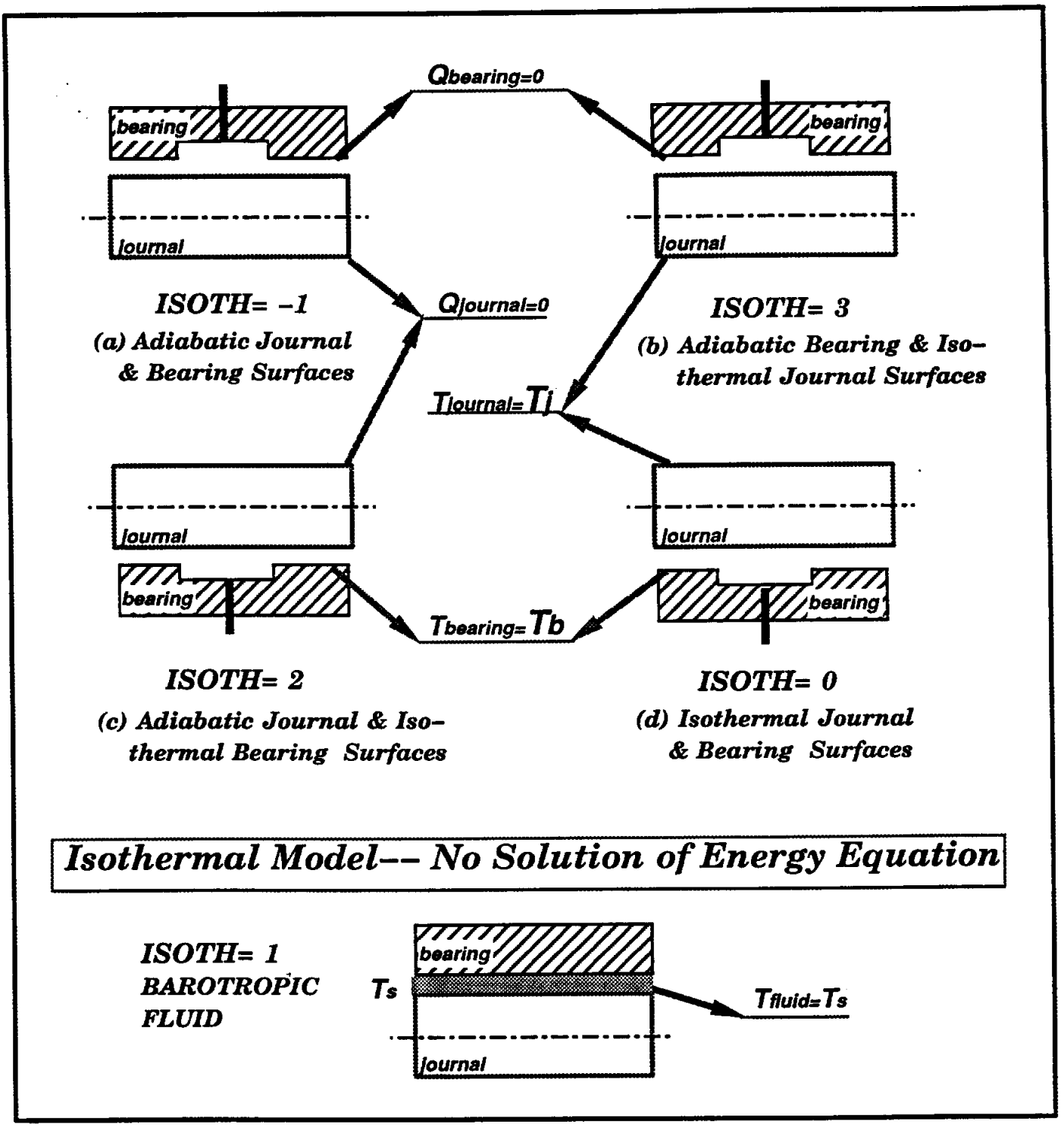

Figure 4. Thermal Models of heat transfer with surface temperature boundary conditions

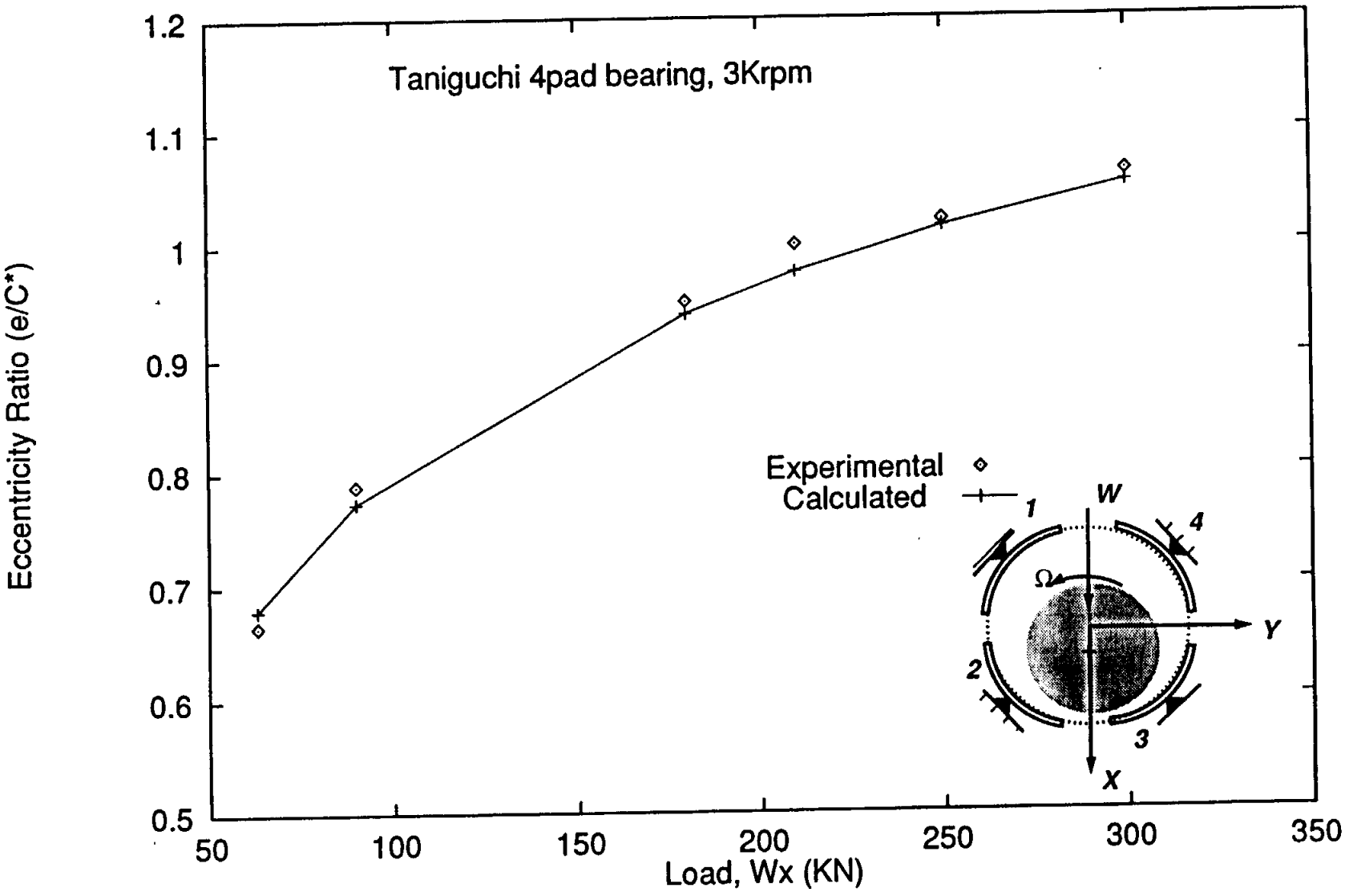

Figure 5. Equilibrium eccentricity vs. applied load
Taniguchi et al. tilt pad bearing. Speed 3krpm

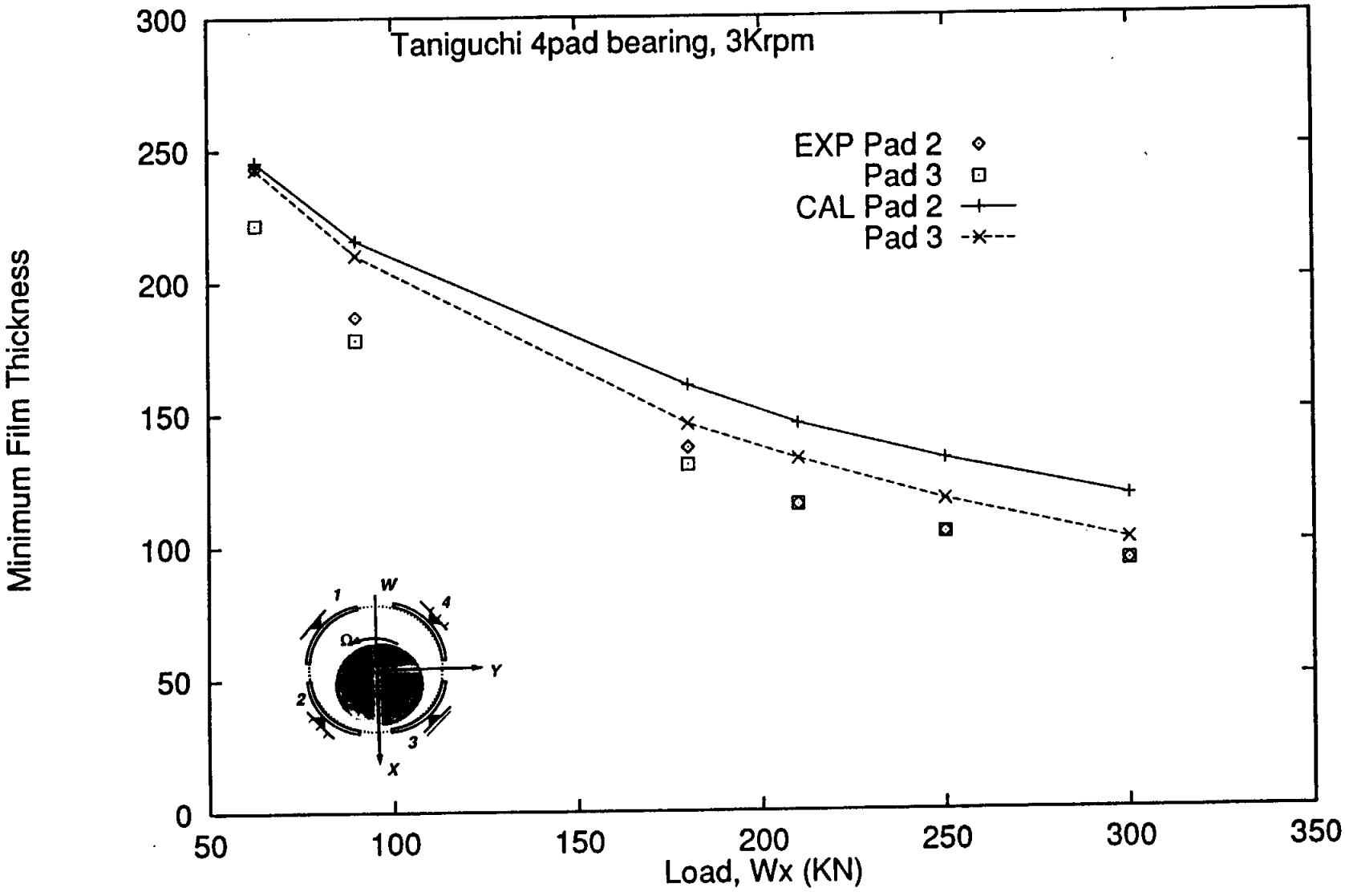

Figure 6. Minimum film thickness (μm) vs. applied load

Taniguchi et al. tilt pad bearing. Speed 3krpm

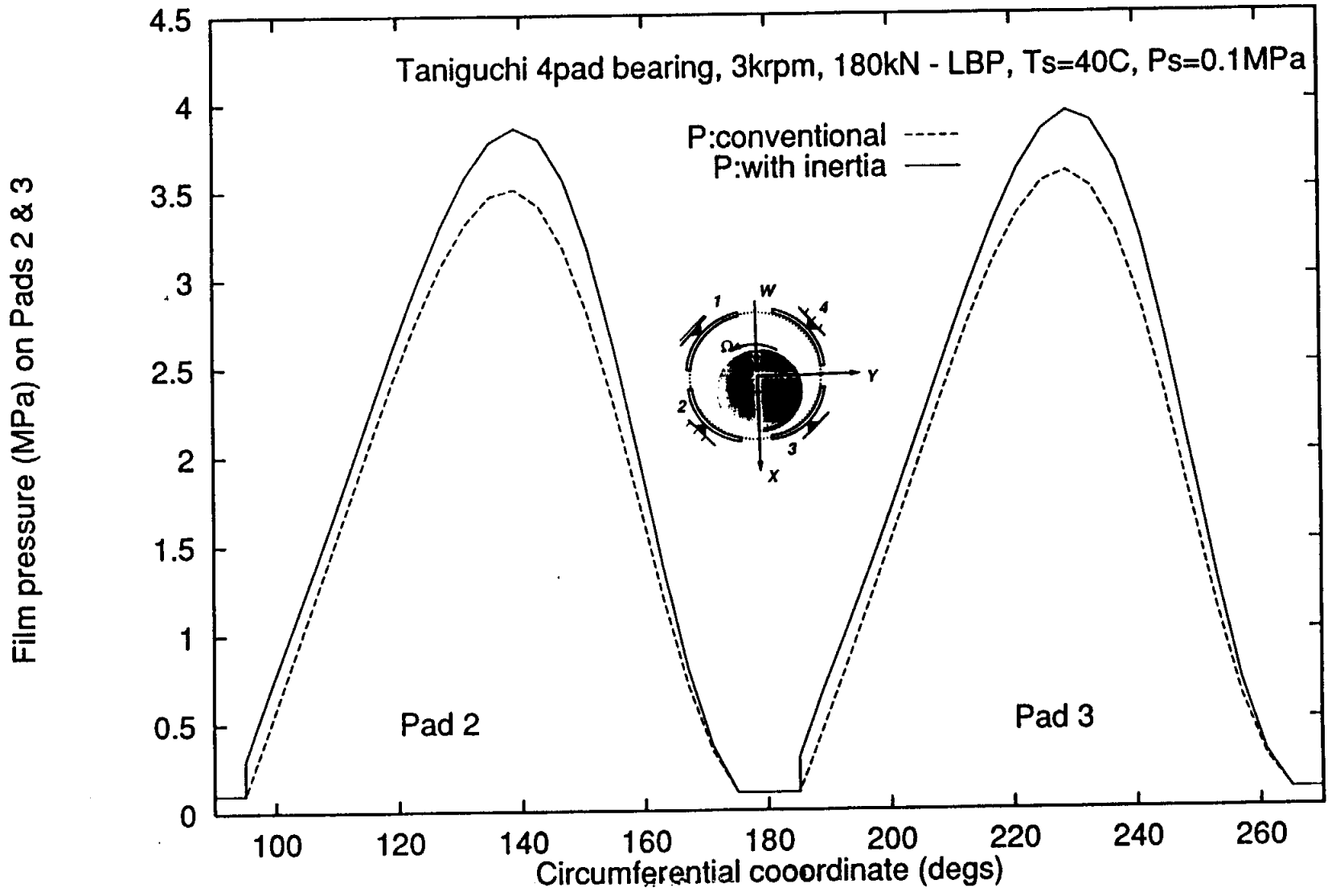

Figure 7. Centerline film pressure (MPa) on loaded pads

Taniguchi et al. tilt pad bearing. Speed 3krpm, Load=180kN

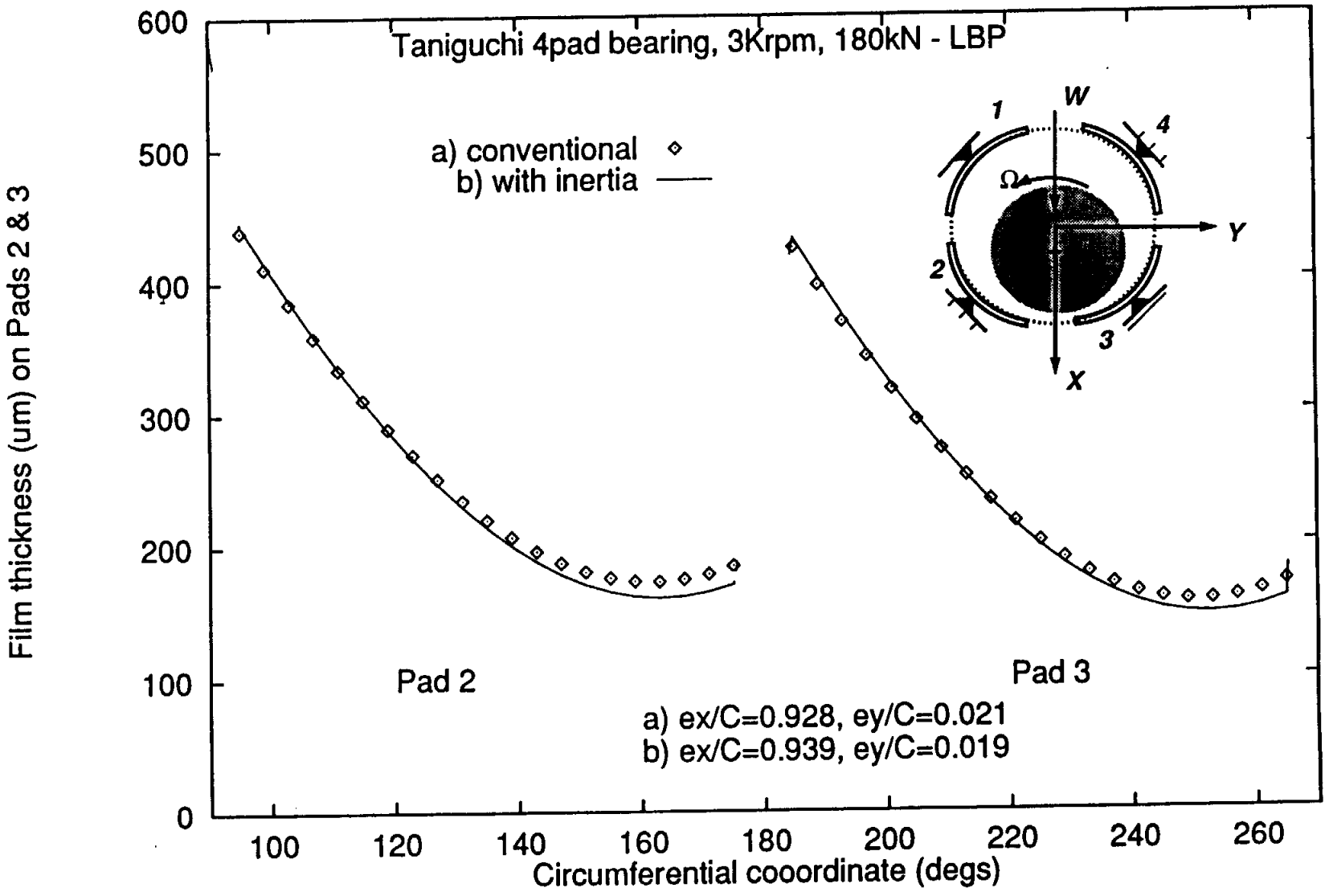

Figure 8. Film thickness (μm) on loaded pads.

Taniguchi et al. tilt pad bearing. Speed 3krpm, Load=180kN

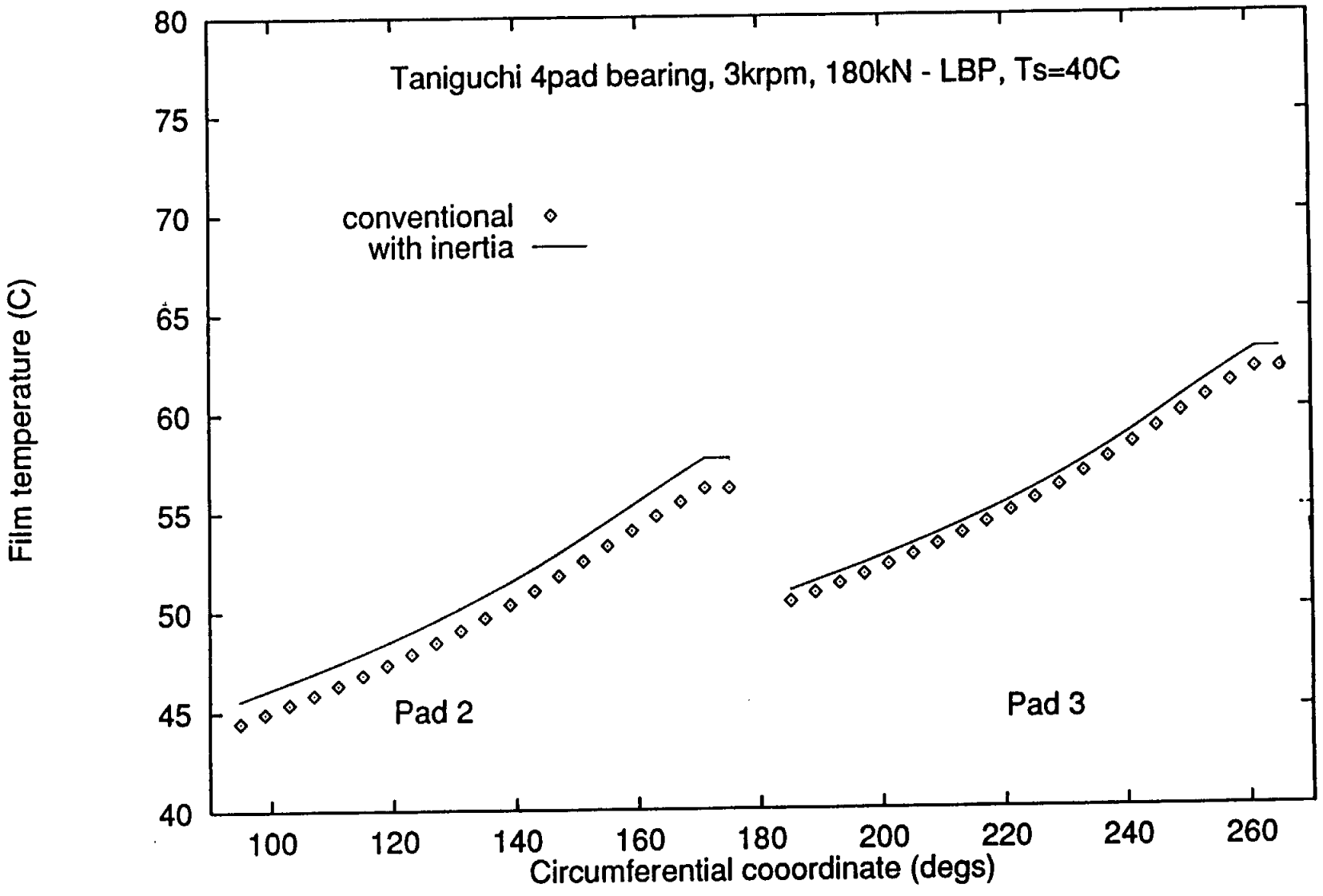

Figure 9. Bulk–flow film temperature on loaded pads.
Taniguchi et al. tilt pad bearing. Speed 3krpm, Load=180kN

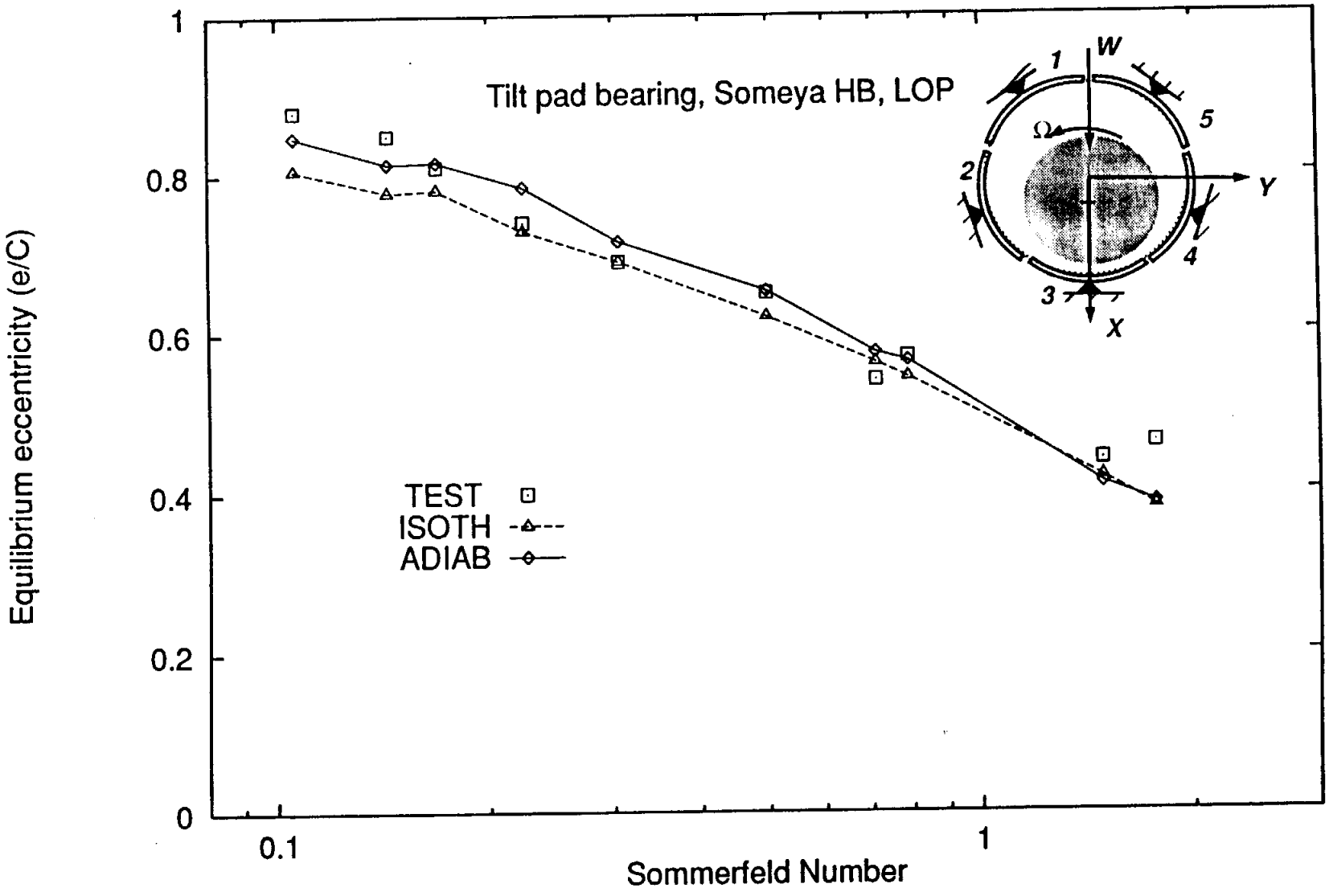

Figure 10. Equilibrium eccentricity vs. Sommerfeld Number

TEST Measurements, ISOthermal and ADIAbatic solutions.
Someya's databook 4 shoe tilt pad bearing – Load on pad

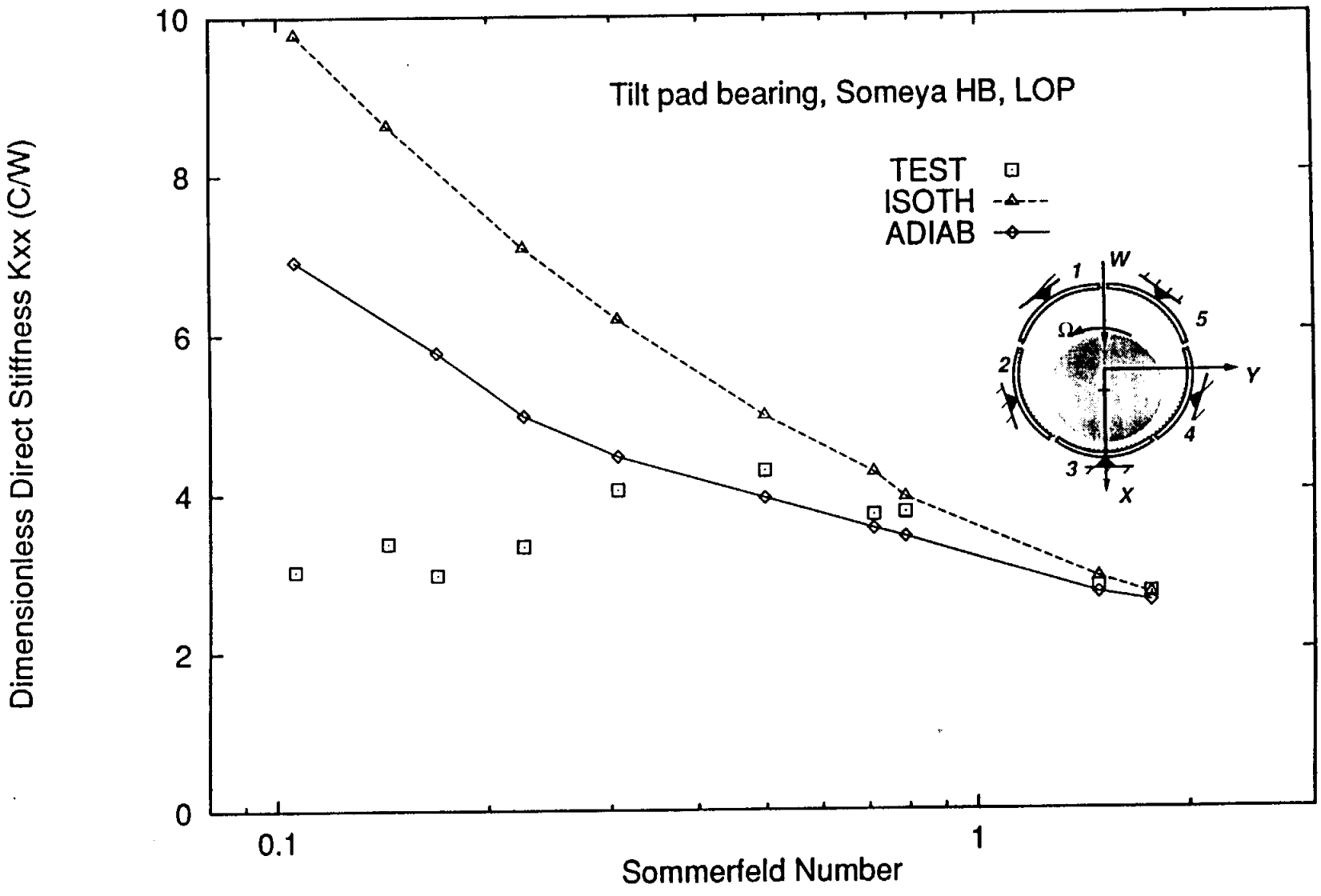

Figure 11. Direct Stiffness Kxx[C/W] vs. Sommerfeld Number

TEST Measurements, ISOthermal and ADIAbatic solutions.
Someya's databook 4 shoe tilt pad bearing – Load on pad

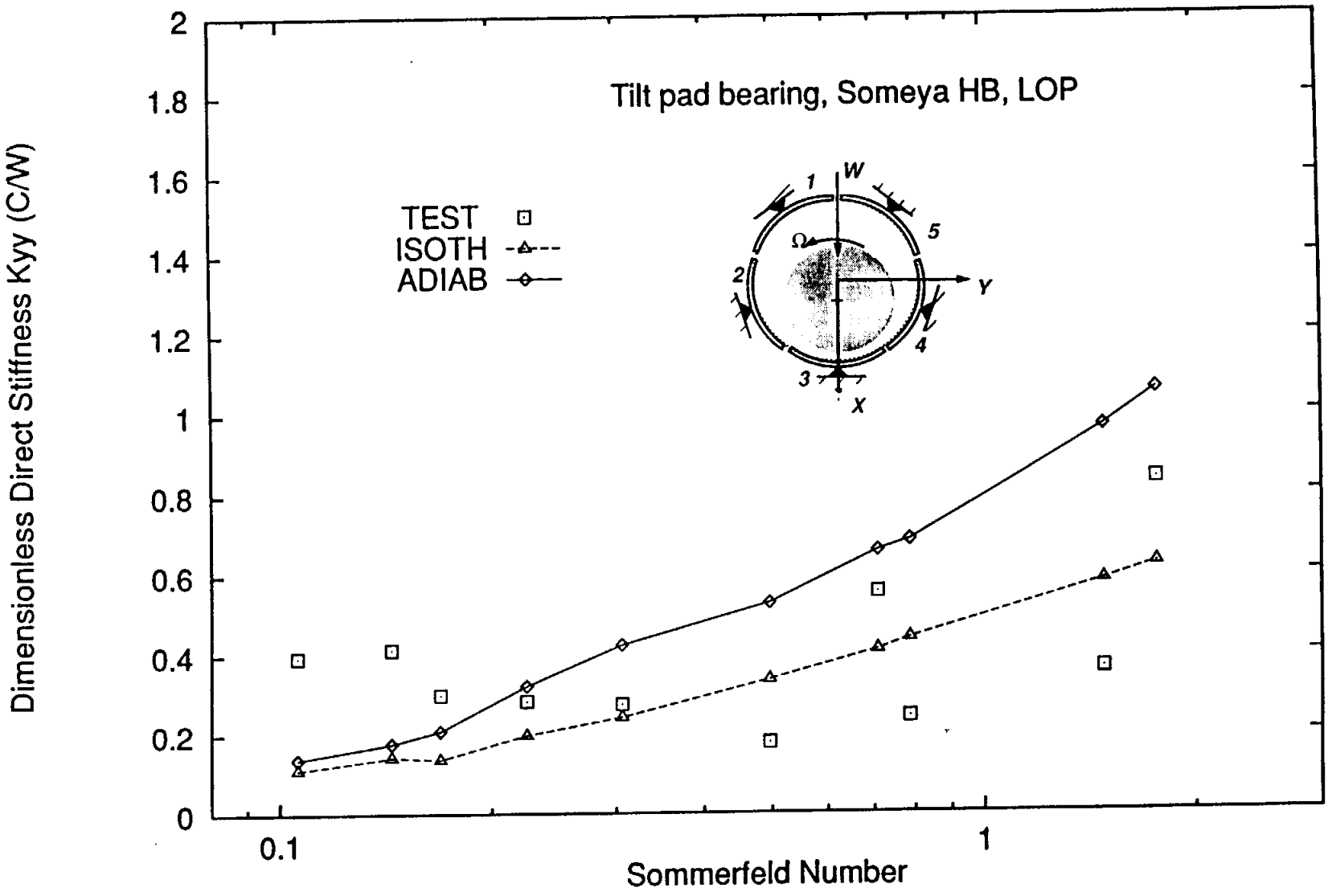

Figure 12. Direct Stiffness K_{YY}[C/W] vs. Sommerfeld Number

TEST Measurements, ISOthermal and ADIAbatic solutions.
Someya's databook 4 shoe tilt pad bearing – Load on pad

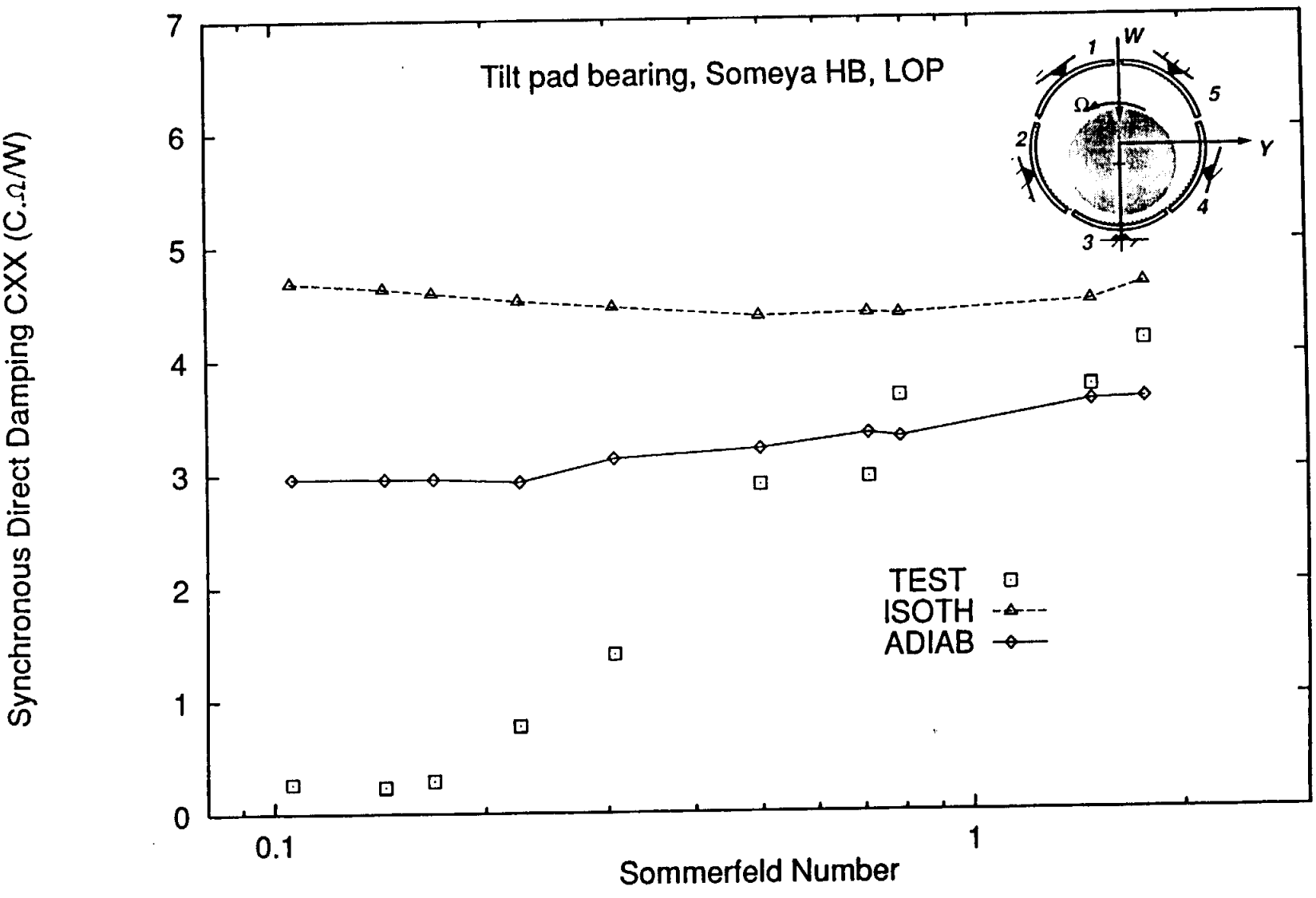

Figure 13. Direct Damping Cxx[CΩ/W] vs. Sommerfeld Number

TEST Measurements, ISOthermal and ADIAbatic solutions.
Someya's databook 4 shoe tilt pad bearing – Load on pad

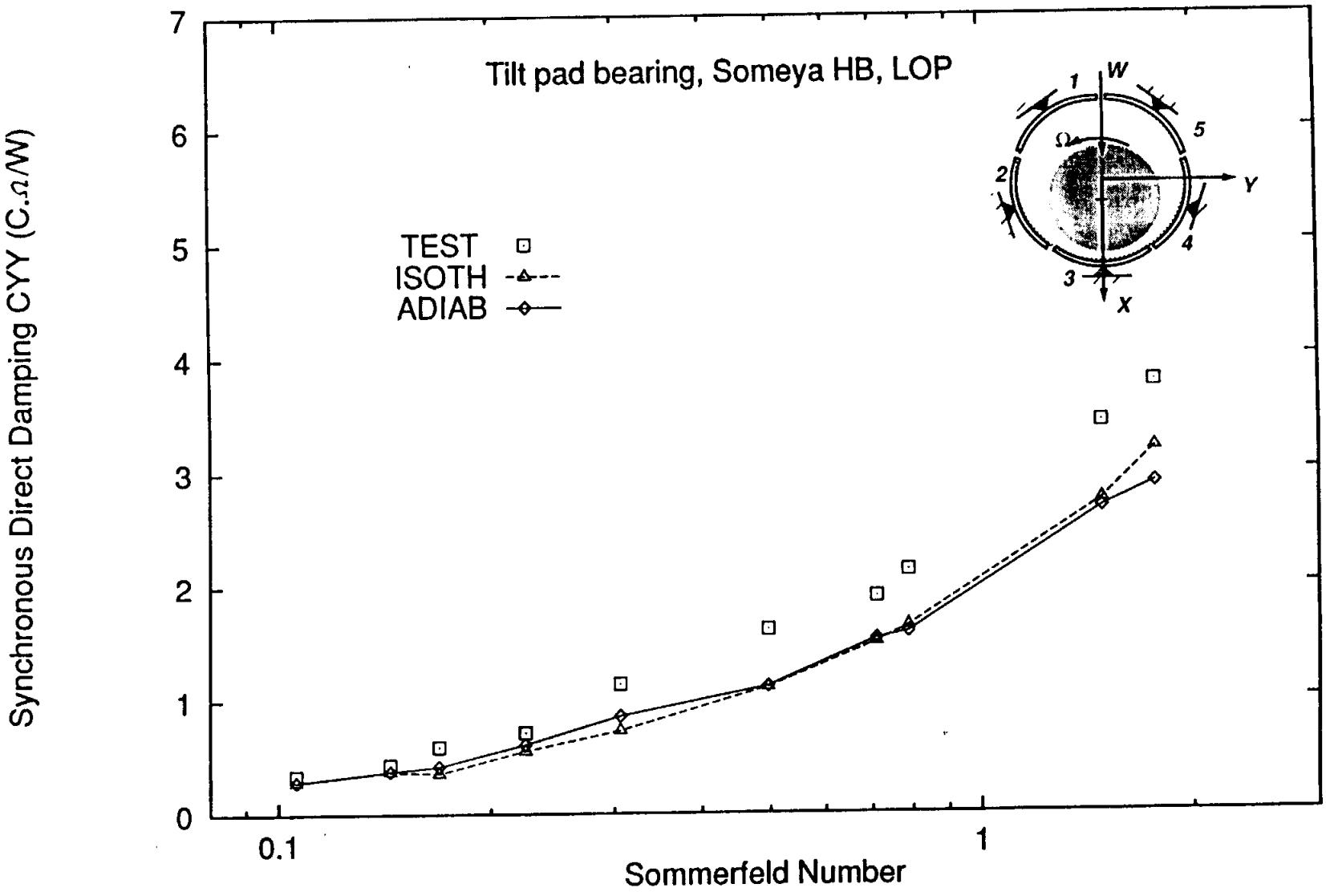

Figure 14. Direct Damping C_{YY}[CΩ/W] vs. Sommerfeld Number

TEST Measurements, ISOthermal and ADIAbatic solutions.
Someya's databook 4 shoe tilt pad bearing – Load on pad

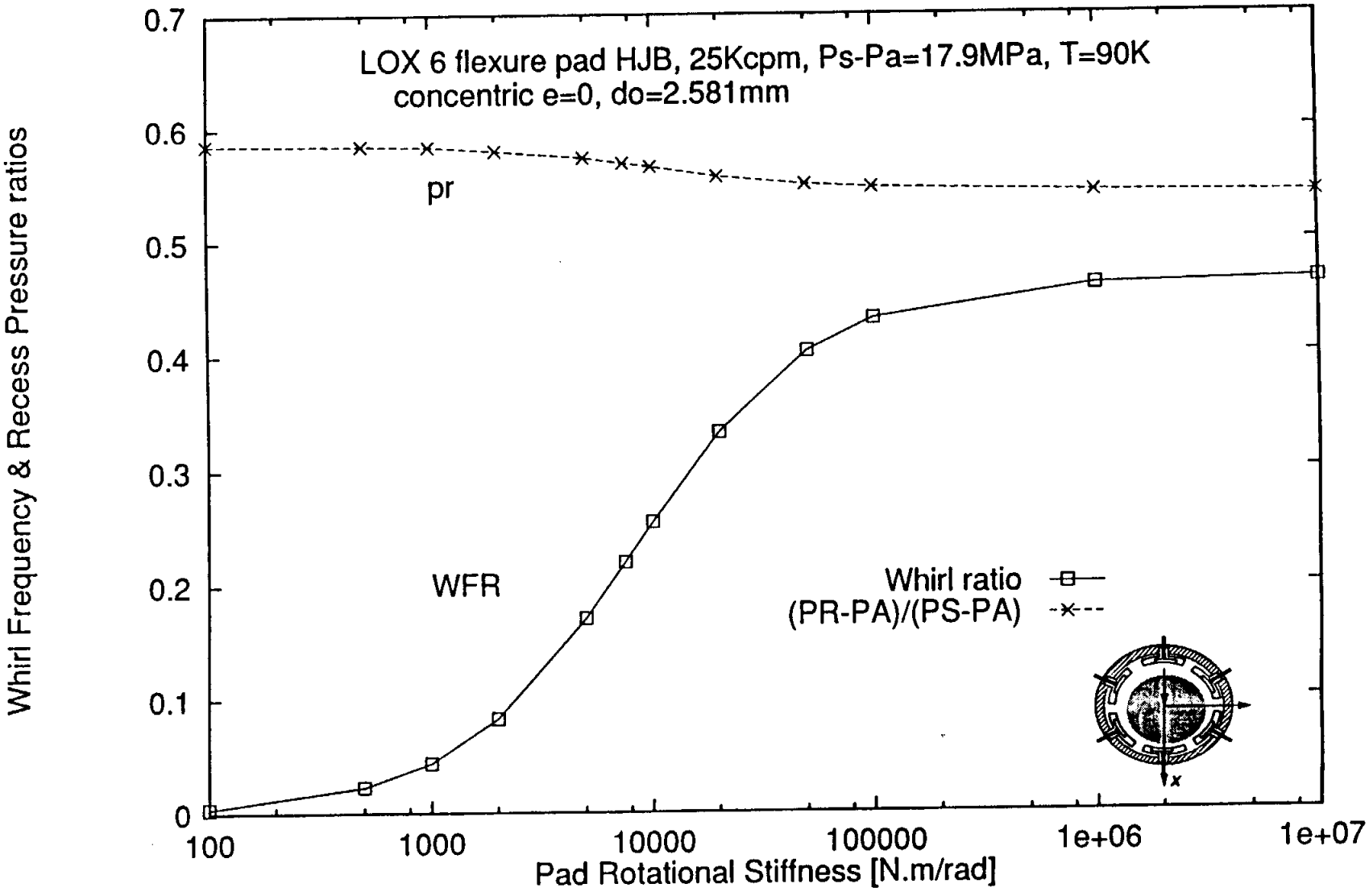

Figure 15. Whirl frequency ratio and recess pressure ratio vs. pad rotational stiffness. LOx flexure-pad hybrid bearing

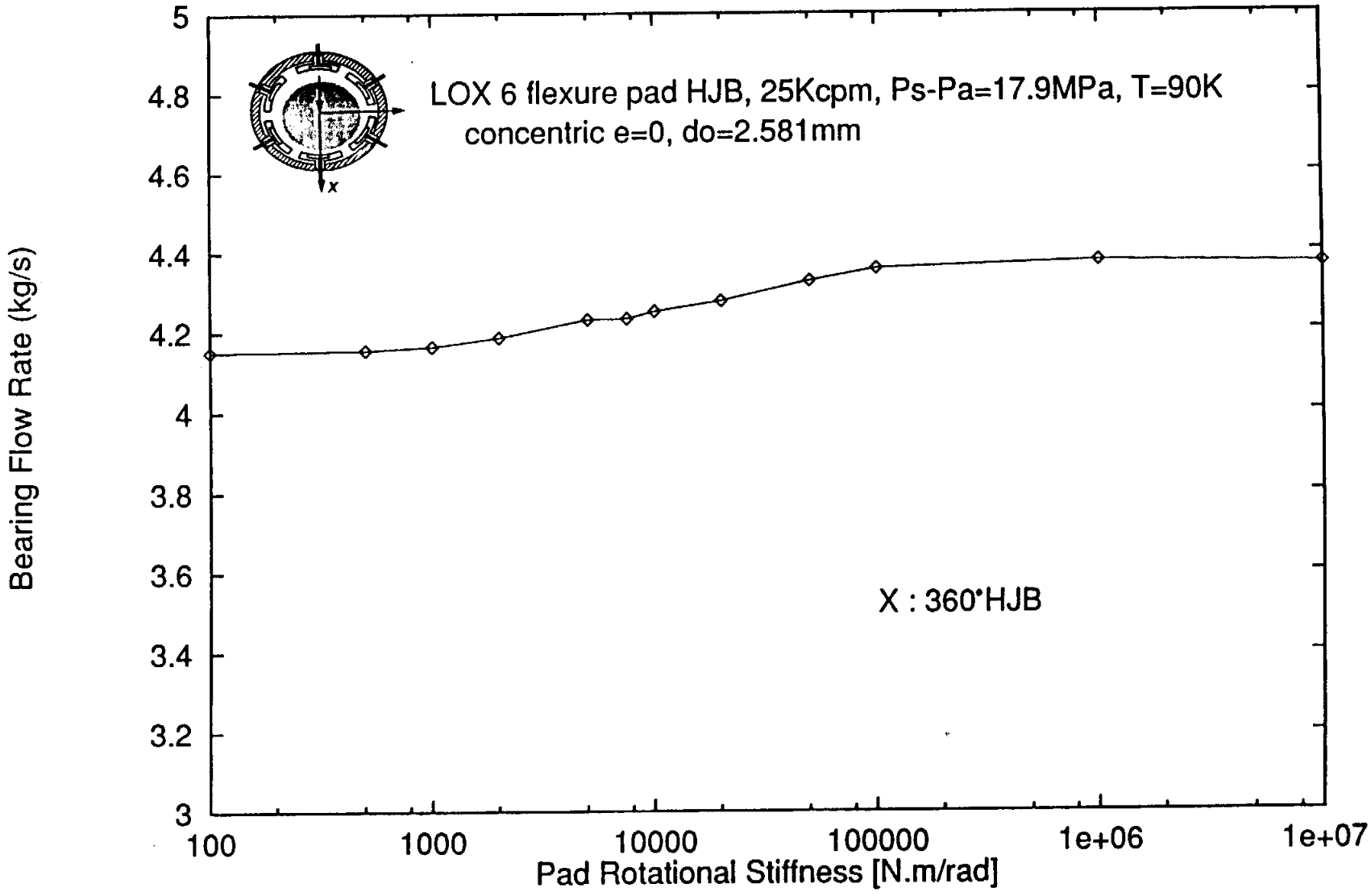

Figure 16. Mass flow rate vs. pad rotational stiffness.

LOx flexure-pad hybrid bearing – concentric operation

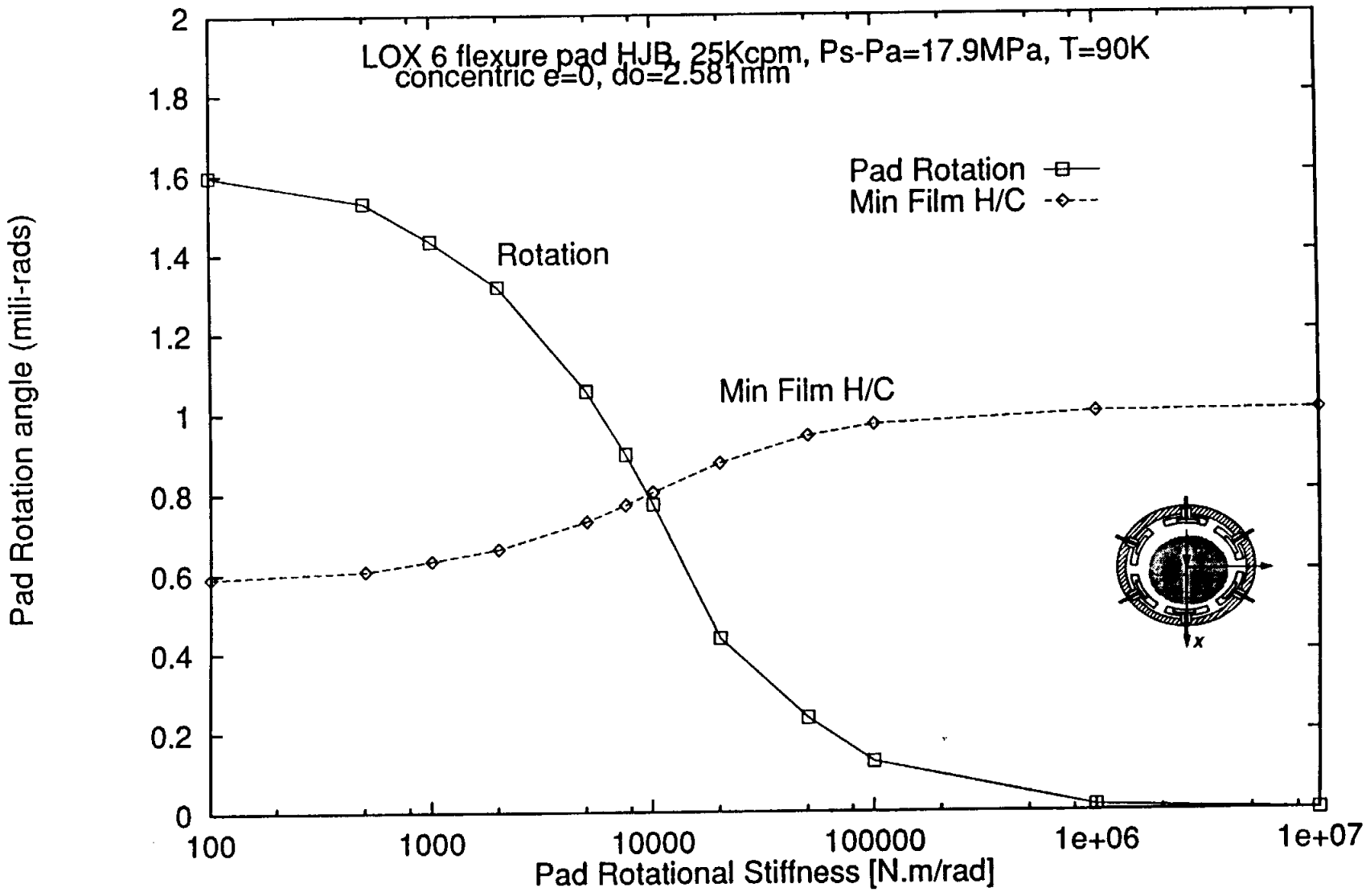

Figure 17. Pad rotation and minimum film thickness vs. pad rotational stiffness. LOx flexure–pad hybrid bearing

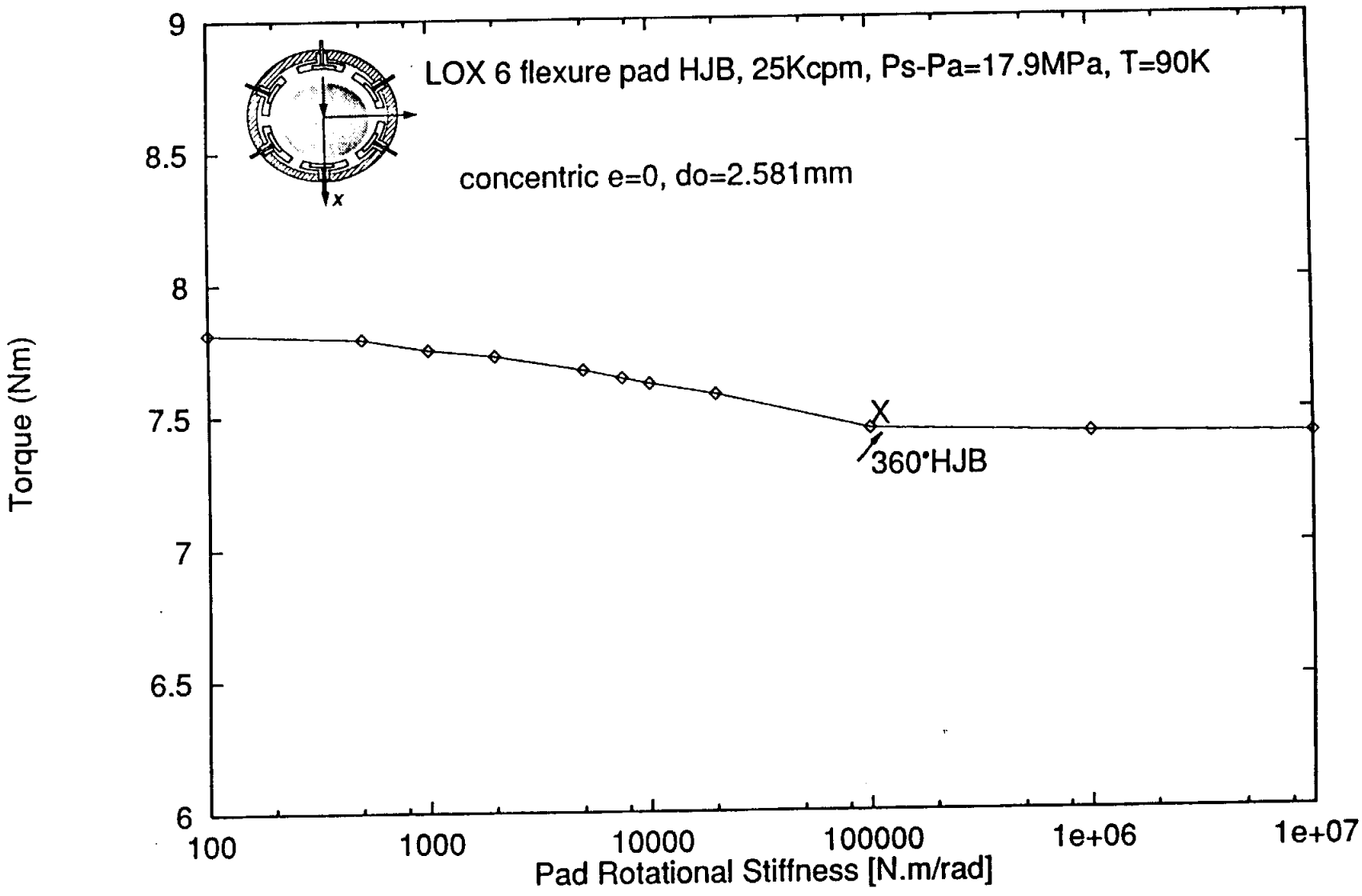

Figure 18. Drag Torque vs. pad rotational stiffness.

LOx flexure-pad hybrid bearing – concentric operation

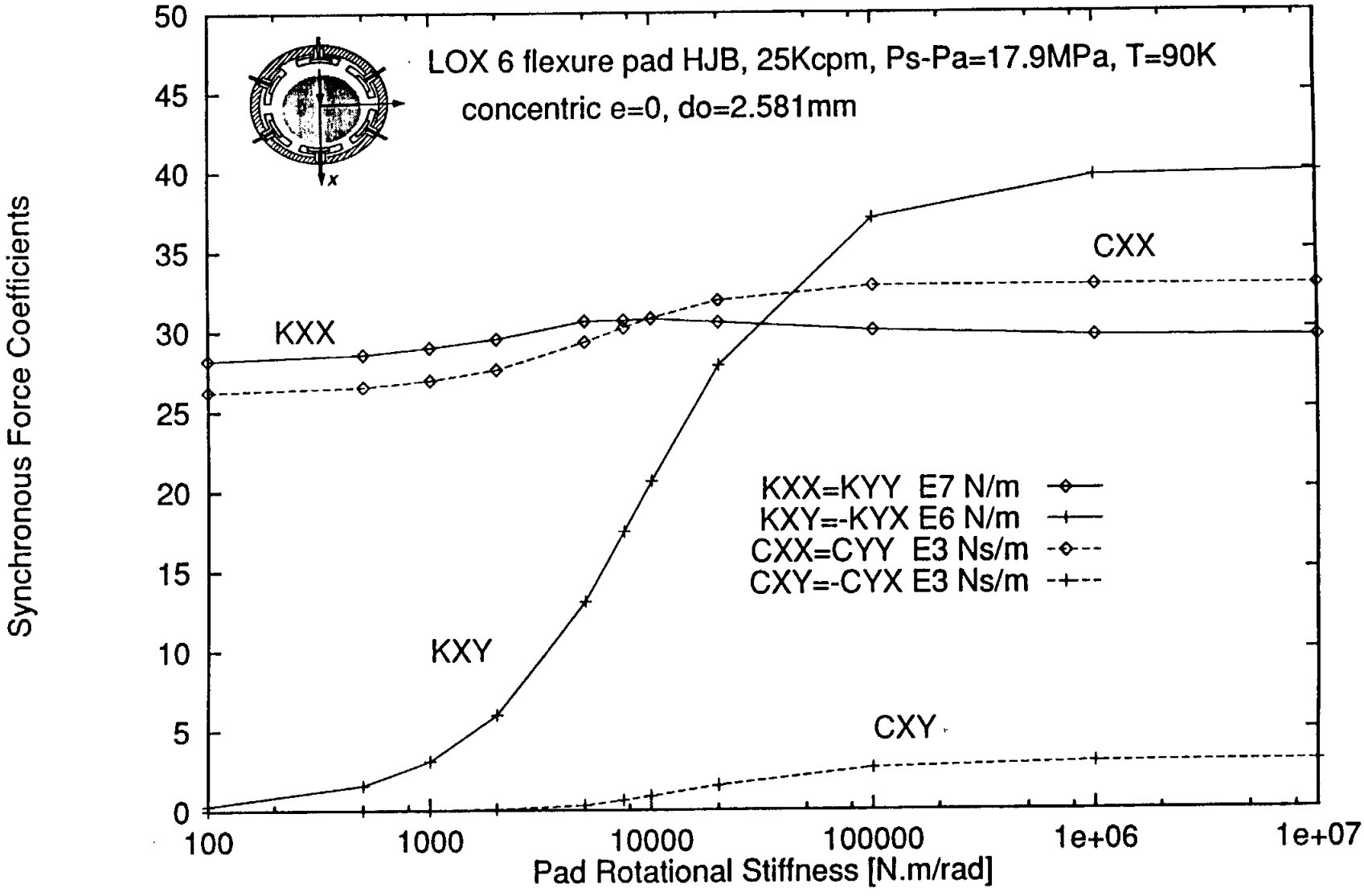

Figure 19. Synchronous force coeffs vs. pad rotational stiffness. **LOx flexure-pad hybrid bearing – concentric**

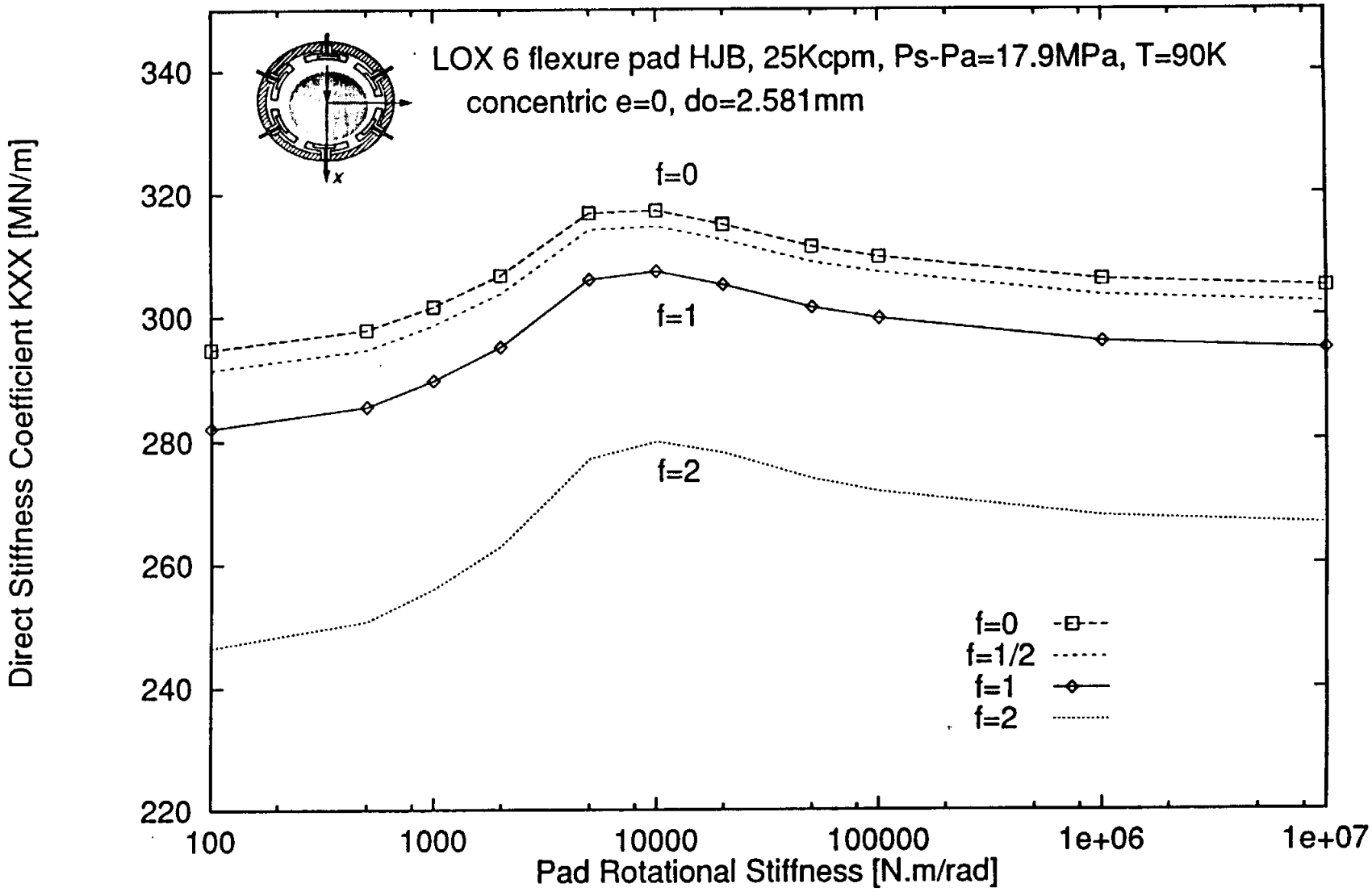

Figure 20. Effect of frequency on direct stiffness KXX=KYY

LOx flexure-pad hybrid bearing - concentric operation

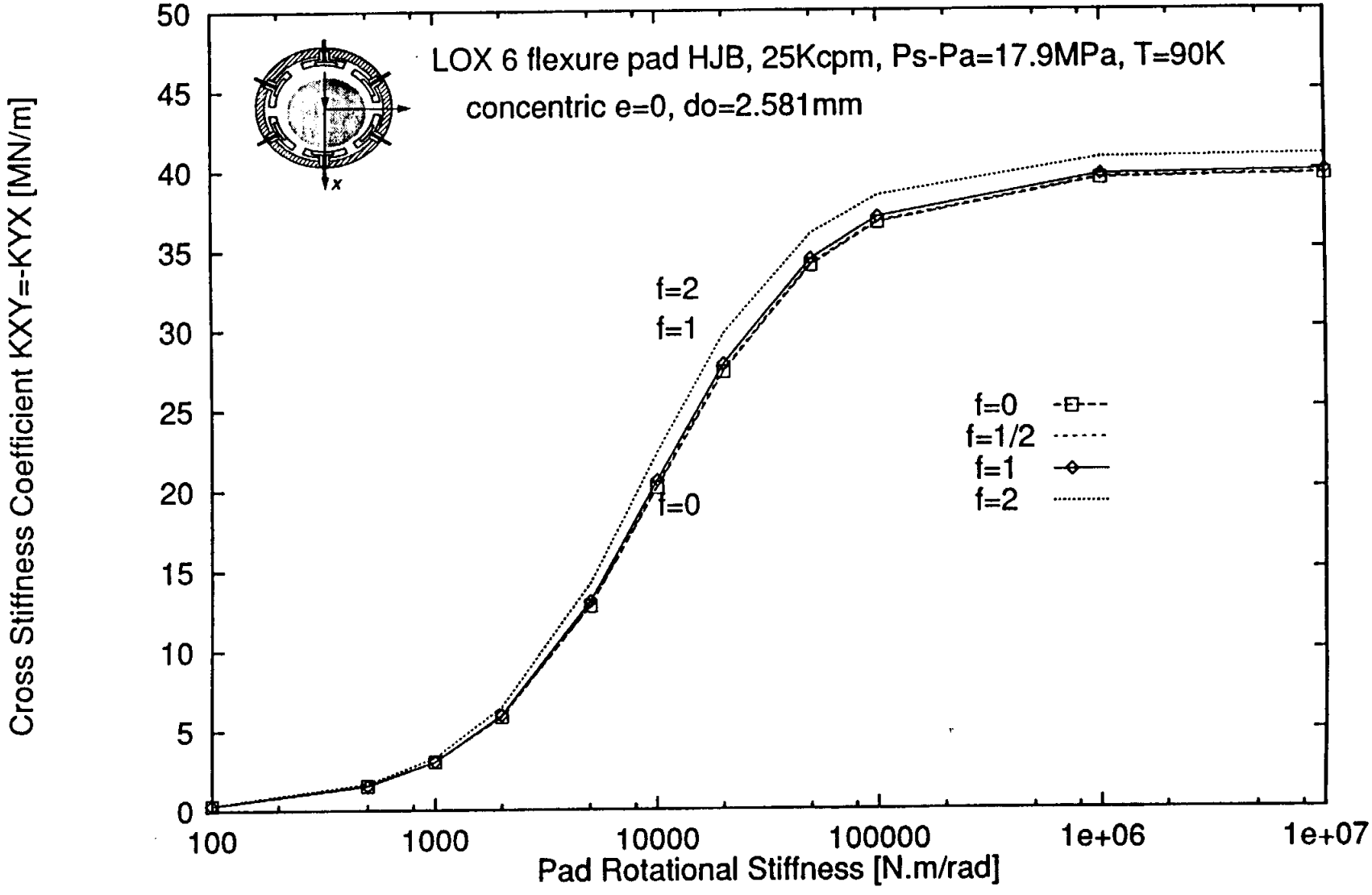

Figure 21. Effect of frequency on cross stiffness $K_{XY}=-K_{YX}$

LOx flexure-pad hybrid bearing – concentric operation

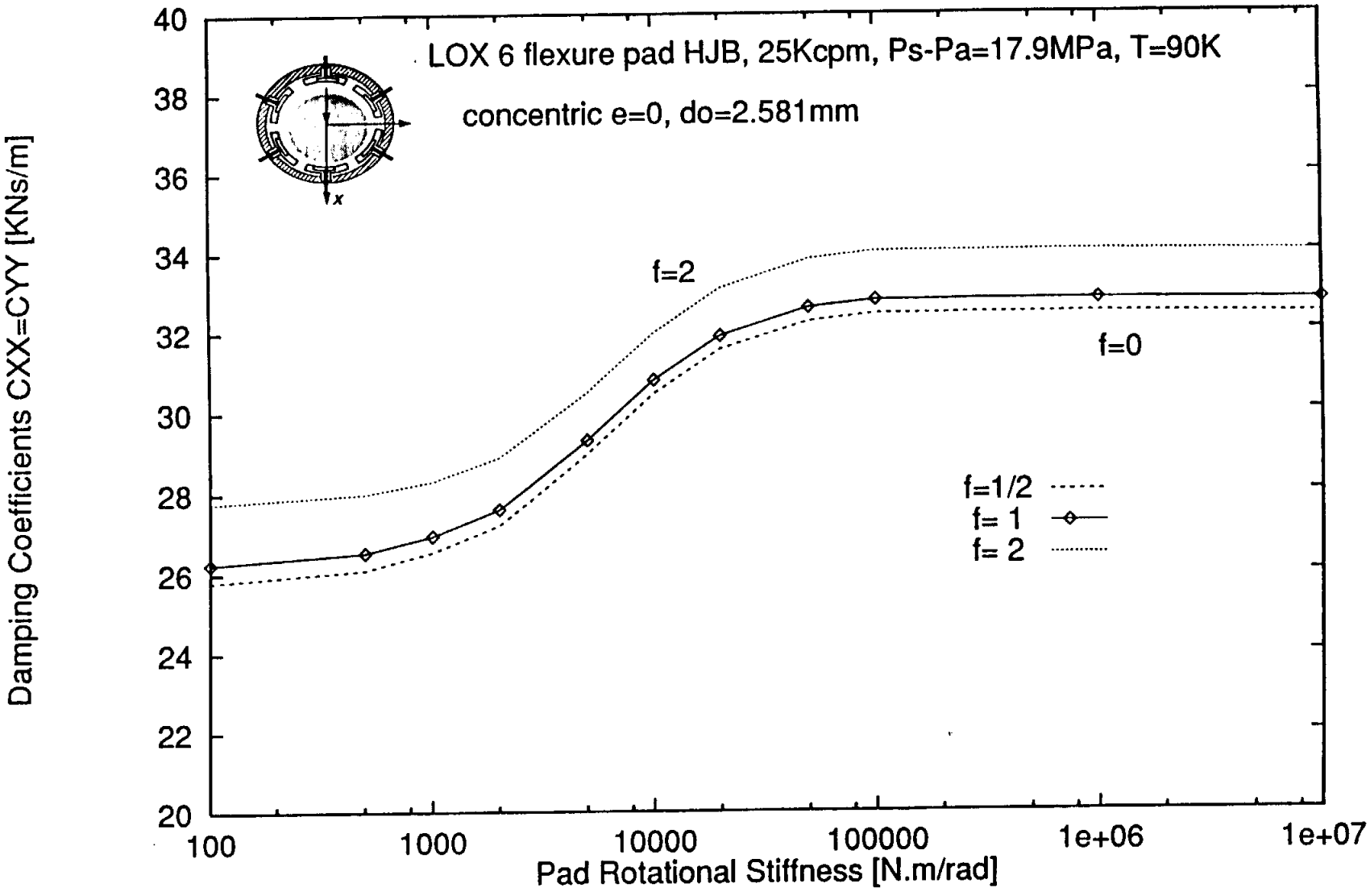

Figure 22. Effect of frequency on direct damping C_{XX}=C_{YY}

LOx flexure-pad hybrid bearing – concentric operation

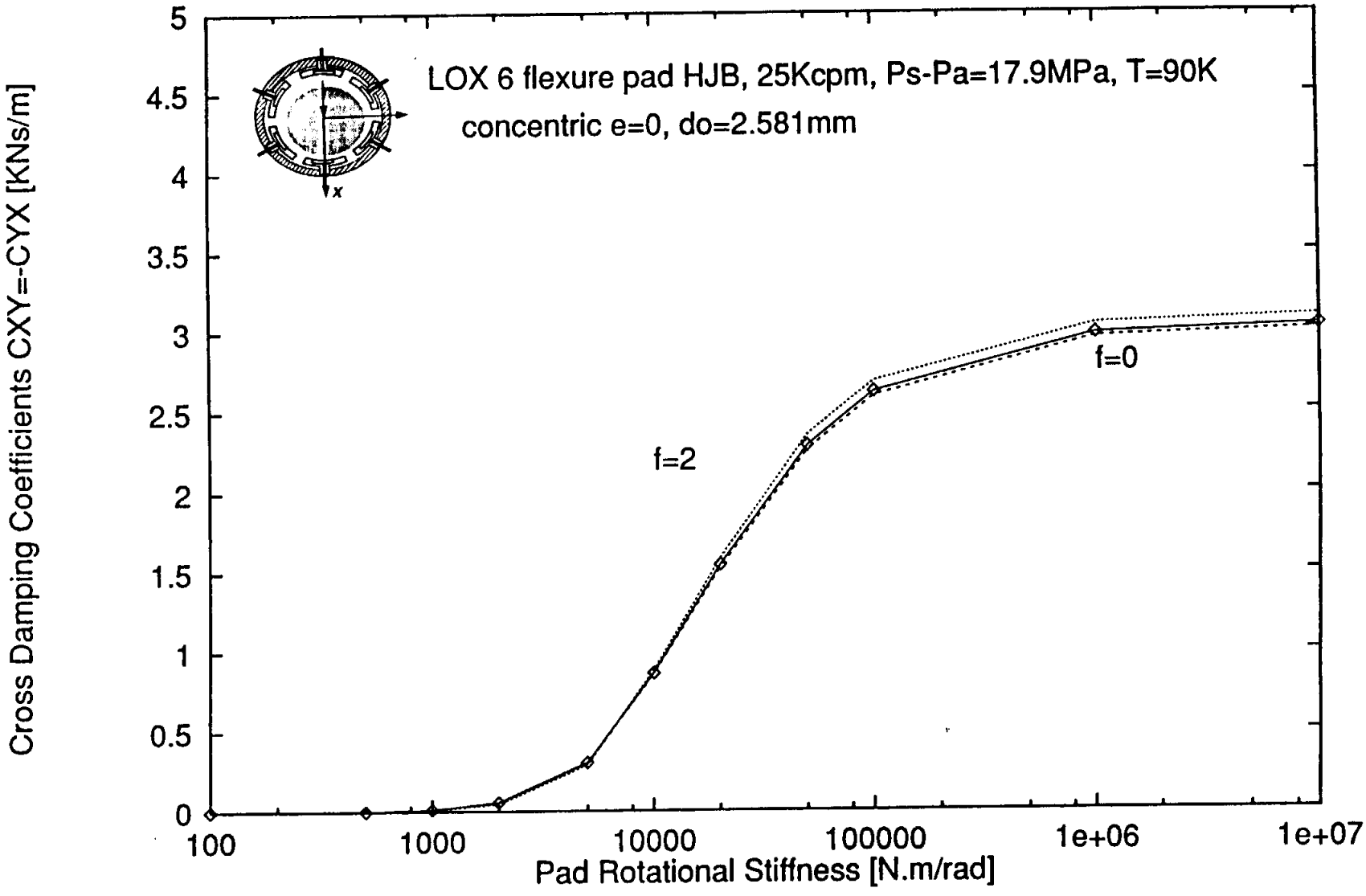

Figure 23. Effect of frequency on cross damping $C_{XY}=-C_{YX}$

LOx flexure-pad hybrid bearing – concentric operation

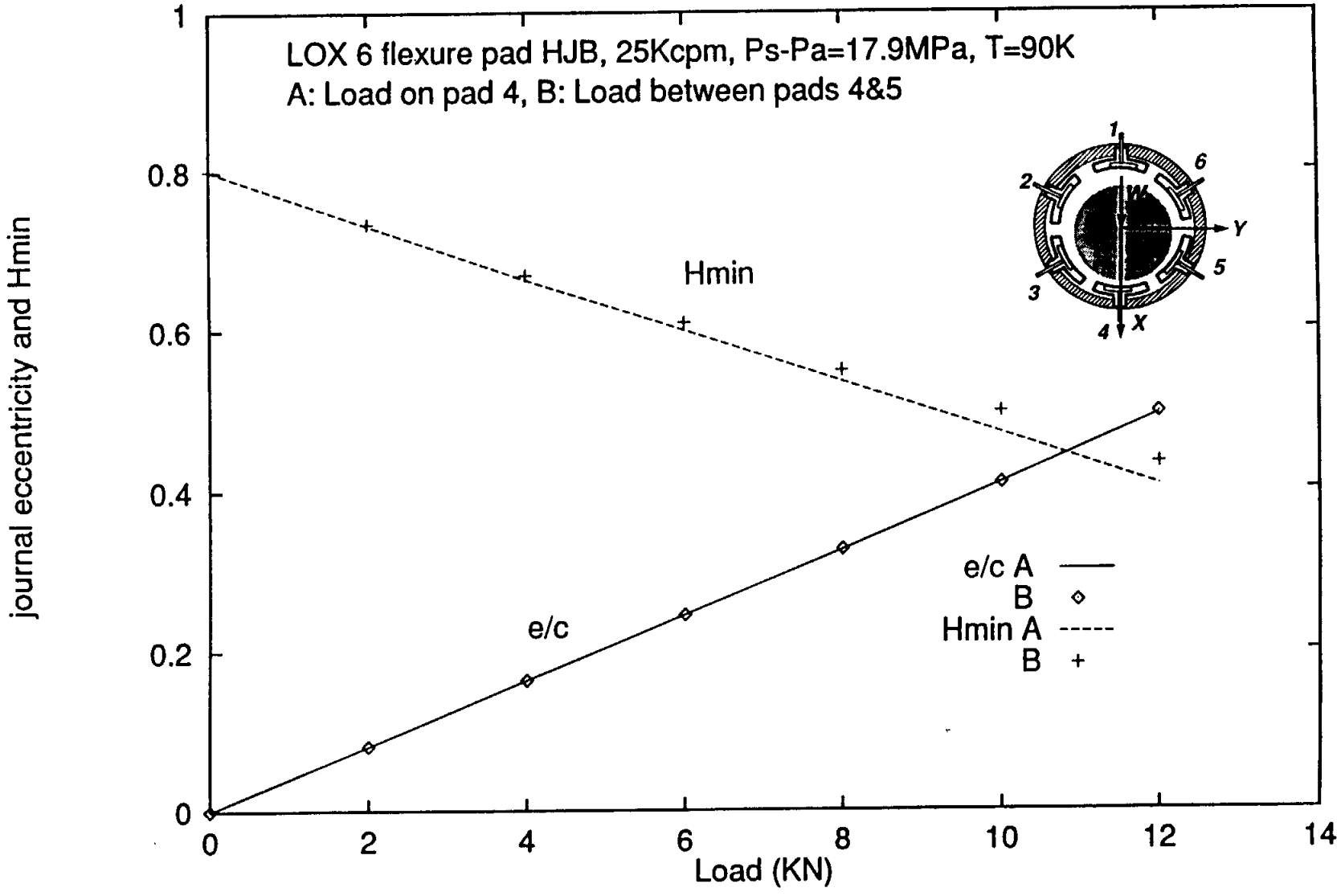

Figure 24. Equilibrium ecentricity vs. load for Kr=10k Nm/rad (A– on pad, B– between pads)

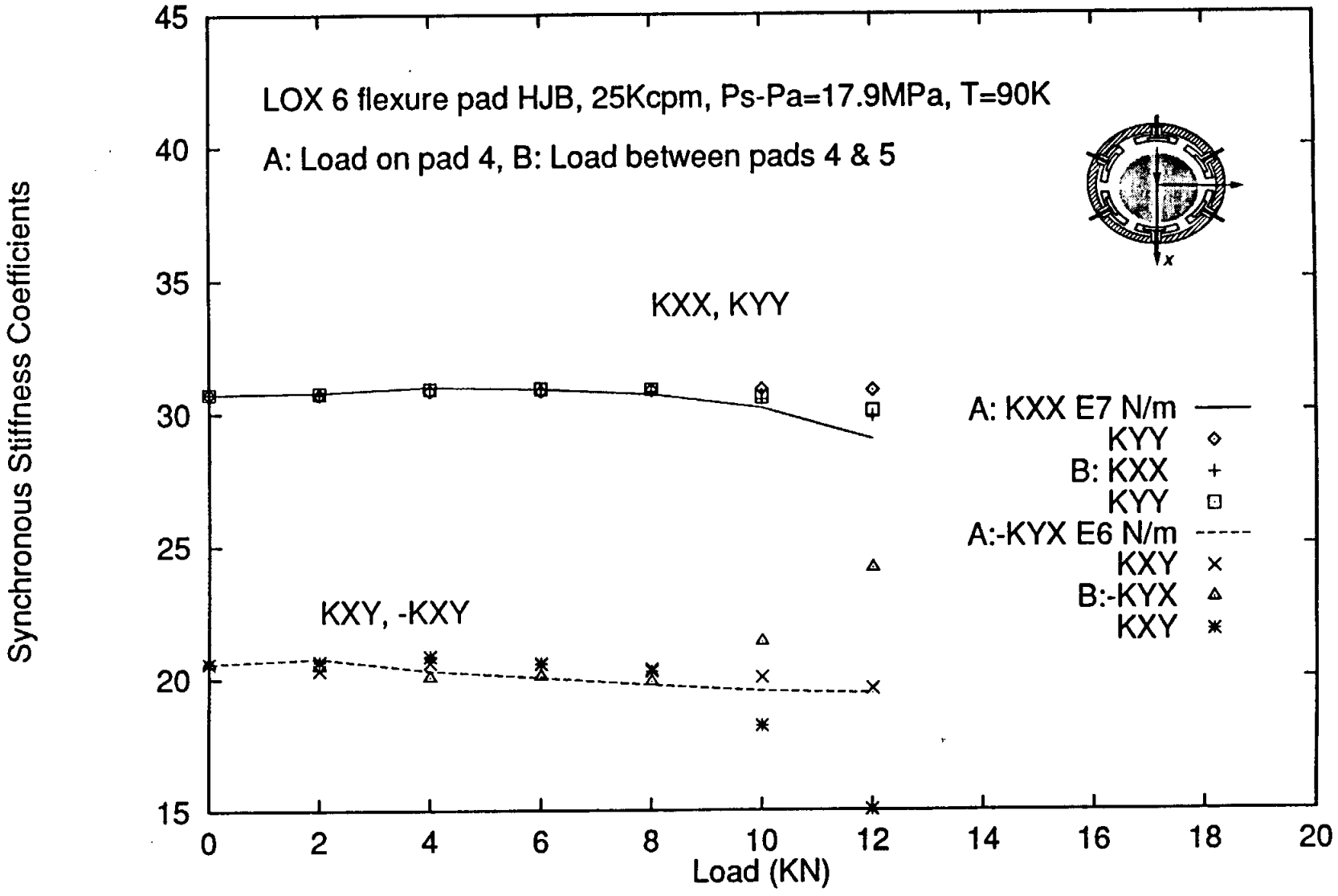

Figure 25. Stiffness Coefficients vs. load for Kr=10k Nm/rad (A– on pad, B– between pads)

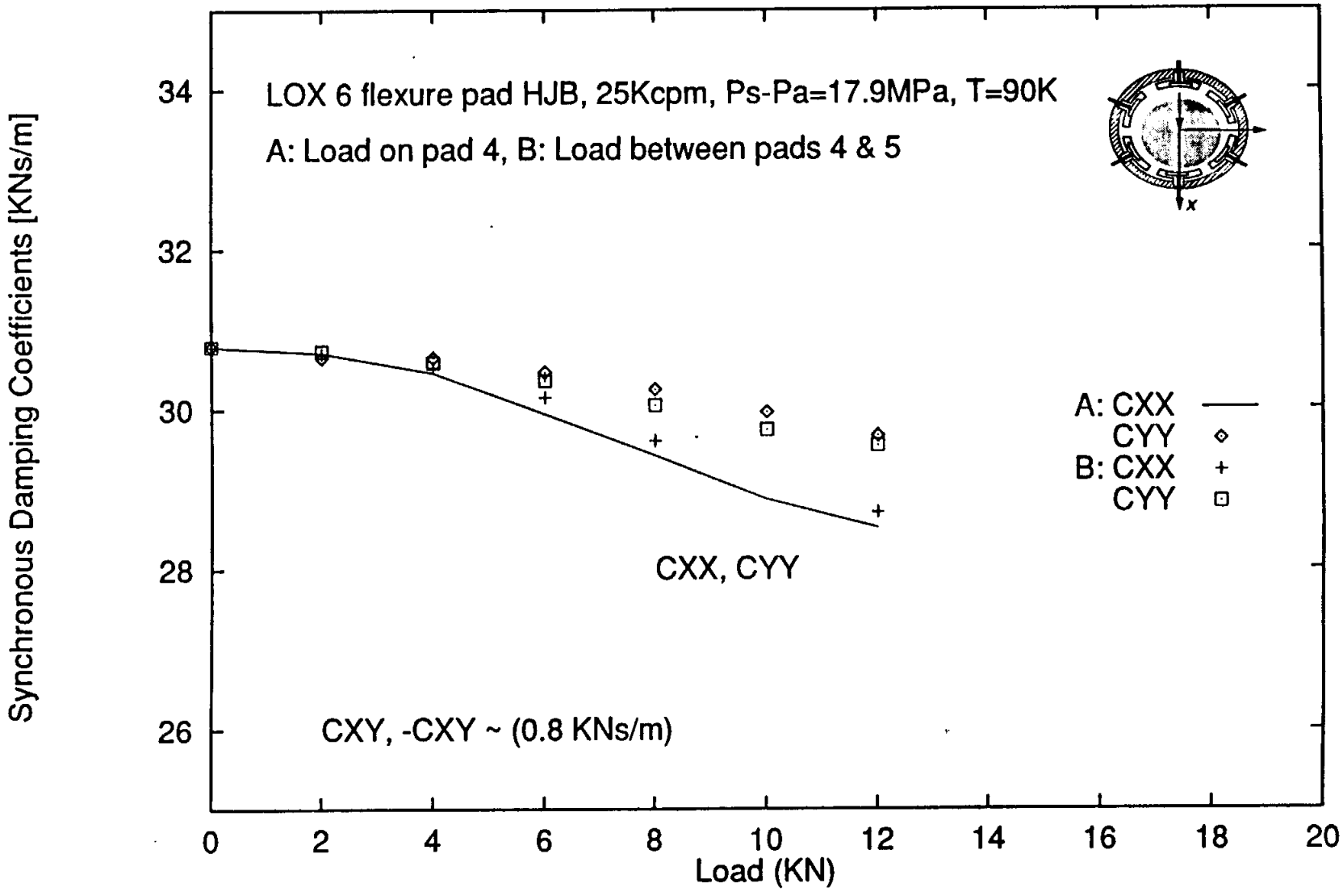

Figure 26. Damping Coefficients vs. load for Kr=10k Nm/rad (A– on pad, B– between pads)

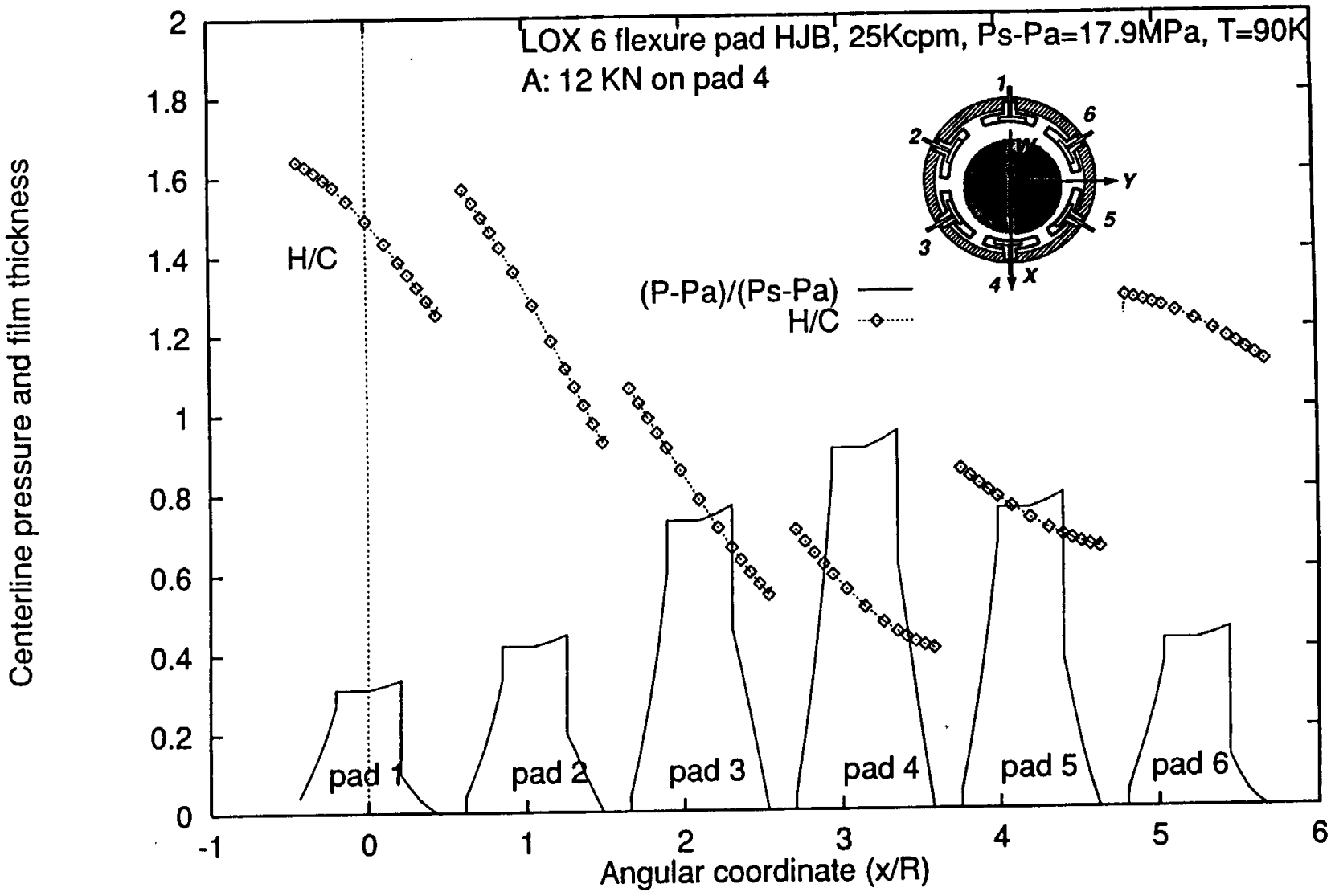

Figure 27. Centerline pressure and film thickness for Kr=10k Nm/rad and 10kN load on pad#4